

# Lattice Q C D at H igh T em perature and D ensity

Frithjof Karsch,

Fakultät für Physik, Universität Bielefeld, D -33615 Bielefeld, Germany

**Abstract:** After a brief introduction into basic aspects of the formulation of lattice regularized QCD at finite temperature and density we discuss our current understanding of the QCD phase diagram at finite temperature. We present results from lattice calculations that emphasize the deconfining as well as chiral symmetry restoring features of the QCD transition, and discuss the thermodynamics of the high temperature phase.

## 1 Introduction

Almost immediately after the ground-breaking demonstration that the numerical analysis of lattice regularized quantum field theories [1] can also provide quantitative results on fundamental non-perturbative properties of QCD [2] it has been realized that this approach will also allow to study the QCD phase transition [3,4] and the equation of state of the quark-gluon plasma [5]. During the last 20 years we have learned a lot from lattice calculations about the phase structure of QCD at finite temperature. In fact, we do understand quite well the thermodynamics in the heavy quark mass limit of QCD, the pure SU(3) gauge theory, and even have calculated the critical temperature and the equation of state in this limit with an accuracy of a few percent. However, it is only now that we start to reach a level of accuracy in numerical calculations of QCD thermodynamics that allows to seriously consider quantitative studies of QCD with a realistic light quark mass spectrum. An important ingredient in the preparation of such calculations is the development of new regularization schemes in the fermion sector of the QCD Lagrangian, which allow to reduce discretization errors and also improve the flavour symmetry of the lattice actions. The currently performed investigations of QCD thermodynamics provide first results with such improved actions and prepare the ground for calculations with a realistic light quark mass spectrum.

The interest in analyzing the properties of QCD under extreme conditions is twofold. On the one hand it is the goal to reach a quantitative description of the behaviour of matter at high temperature and density. This does provide important input for a quantitative description of experimental signatures for the occurrence of a phase transition in heavy ion collisions and should also help to understand better the phase transitions that occurred during the early times of the evolution of the universe. Eventually it also may allow to answer the question whether a quark-gluon plasma can exist in the interior of dense neutron stars or did exist in early stages of supernova explosions. For this reason one would like to reach a quantitative understanding of the QCD equation of state, determine critical parameters such as the critical temperature and the critical energy density and predict

the modification of basic hadron properties (masses, decay widths) with temperature. On the other hand the analysis of a complicated quantum field theory like QCD at non-zero temperature can also help to improve our understanding of its non-perturbative properties at zero temperature. The introduction of external control parameters (temperature, chemical potential) allows to observe the response of different observables to this and may provide a better understanding of their interdependence [6]. As such one would, for instance, like to clarify the role of confinement and chiral symmetry breaking for the QCD phase transition. In which respect is the QCD phase transition deconfining and/or chiral symmetry restoring? In how far can the critical behaviour be described by intuitive pictures based on percolation, bag or resonance gas models which have been developed for the QCD transition? We will discuss these qualitative aspects of the QCD thermodynamics and also present results on basic questions concerning the equation of state and the critical temperature of the transition which ask for quantitative answers.

In the next section we give a short introduction into the lattice formulation of QCD thermodynamics. In Section 3 we discuss the basic structure of the QCD phase diagram at finite temperature as it is known from lattice calculations. Section 4 is devoted to a discussion of basic thermodynamic observables which characterize the QCD transition to the plasma phase and we will identify general properties which show the deconfining and chiral symmetry restoring features of this transition. In Section 5 we comment on different length scales characterizing the QCD plasma and try to establish the temperature regime where lattice calculations may make contact with perturbative approaches. A description of recent results on the QCD equation of state and the critical temperature of the QCD transition which emphasizes the quark mass and flavour dependence of these quantities is given in Sections 6 and 7, respectively. A brief discussion of the problems arising in lattice formulations of QCD at non-zero baryon number density or chemical potential is given in Section 8. Finally we give our conclusions in Section 9 and describe a specific set of improved gauge and fermion lattice actions in an Appendix.

## 2 The Lattice Formulation of QCD Thermodynamics

### 2.1 The basic steps from continuum to lattice ...

Starting point for the discussion of the equilibrium thermodynamics of QCD on the lattice is the QCD partition function, which explicitly depends on the volume ( $V$ ), the temperature ( $T$ ) and the quark number chemical potential ( $\mu$ ). It is represented in terms of a Euclidean path integral over gauge ( $A$ ) and fermion ( $\psi$ ;  $\bar{\psi}$ ) fields,

$$Z(V; T; \mu) = \int \mathcal{D}A \mathcal{D}\psi \mathcal{D}\bar{\psi} e^{-S_E(V; T; \mu)} \quad (1)$$

where  $A$  and  $\psi$  obey periodic and anti-periodic boundary conditions in Euclidean time, respectively. The Euclidean action  $S_E = S_G + S_F$  contains a purely gluonic contribution ( $S_G$ ) expressed in terms of the field strength tensor,  $F_{\mu\nu} = \partial_\mu A_\nu - \partial_\nu A_\mu - ig[A_\mu, A_\nu]$ , and a fermion part ( $S_F$ ), which couples the gauge and fermions field through the standard minimal substitution,

$$S_E(V; T; \mu) = S_G(V; T) + S_F(V; T; \mu) \quad (2)$$

$$S_G(V;T) = \int_0^T dx_0 \int_V d^3x \frac{1}{2} \text{Tr} F_{\mu\nu} F_{\mu\nu} \quad (3)$$

$$S_F(V;T; \{m_f\}) = \int_0^T dx_0 \int_V d^3x \sum_{f=1}^{n_f} \bar{\psi}_f (i \not{D} - m_f) \psi_f \quad (4)$$

Here  $m_f$  are the different quark masses for the  $n_f$  different quark flavours and  $g$  denotes the QCD coupling constant.

The path integral appearing in Eq. 1 is regularized by introducing a four dimensional space-time lattice of size  $N^3 \times N$  with a lattice spacing  $a$ . Volume and temperature are then related to the number of points in space and time directions, respectively,

$$V = (N a)^3 ; \quad T^{-1} = N a \quad (5)$$

While the discretization of the fermion sector, at least on the naive level, is straightforwardly achieved by replacing derivatives by finite differences, the gauge sector is a bit more involved. Here we introduce link variables  $U_\mu(x)$  which are associated with the link between two neighbouring sites of the lattice and describe the parallel transport of the field  $A$  from site  $x$  to  $x + \hat{\mu}a$ ,

$$U_{x;\mu} = P \exp \left( i g \int_x^{x+\hat{\mu}a} dx^\mu A_\mu(x) \right) \quad (6)$$

where  $P$  denotes the path ordering. The link variables  $U_\mu(x)$  are elements of the  $SU(3)$  colour group. A product of these link variables around an elementary plaquette may be used to define an approximation to the gauge action,

$$\begin{aligned} W_{n;\mu\nu}^{(1;1)} &= \frac{1}{3} \text{Re} \left[ \text{Tr} U_{n;\mu} U_{n+\hat{\mu};\nu} U_{n+\hat{\mu}\hat{\nu}}^\dagger U_{n;\nu}^\dagger \right] \\ &= \frac{g^2 a^4}{2} F^{\mu\nu} F_{\mu\nu} + O(a^6) \quad (7) \end{aligned}$$

A discretized version of the Euclidean gauge action, which reproduces the continuum version up to cut-off errors of order  $a^2$ , thus is given by the Wilson action [1],

$$S_G = \sum_{n=0}^N \sum_{\mu < \nu}^3 W_{n;\mu\nu}^{(1;1)} = \int d^4x L_E + O(a^2) \quad (8)$$

where we have introduced the gauge coupling  $\beta = 6/g^2$ .

As is well-known the naive discretization of the fermionic part of the action, which is obtained by introducing the simple finite difference scheme to discretize the derivative appearing in the fermion Lagrangian, i.e.  $\partial_\mu \psi(x) = (\psi_{n+\hat{\mu}} - \psi_{n-\hat{\mu}})/2a$ , does in the continuum limit not reproduce the particle content one started with. The massless lattice fermion propagator has poles not only at zero momentum but also at all other corners of the Brillouin zone and thus generates 16 rather than a single fermion species in the continuum limit. One thus faces a severe species doubling problem. The way out has been to either introduce an explicit chiral

symmetry breaking term, which is proportional to  $a^2 \bar{\psi} \psi(x)$  and thus vanishes in the continuum limit (Wilson fermions [1]), or to distribute the components of the fermion Dirac spinors over several lattice sites (staggered fermions) [7]. The staggered fermion formulation does not eliminate the species doubling problem completely. One still gets four degenerate fermion species. However, it has the advantage that it preserves a continuous subgroup of the original global chiral symmetry. In the massless limit the chiral condensate thus still is an order parameter for the occurrence of a phase transition at finite temperature.

Progress has been made in formulating lattice QCD also with chiral fermion actions which do avoid the species doubling and at the same time preserve the chiral symmetry of the QCD Lagrangian. This can, for instance, be achieved by introducing an extra fifth dimension [8]. At present, however, very little has been done to study QCD thermodynamics on the lattice with these actions [9]. Much more is known on the QCD thermodynamics from calculations with Wilson and staggered fermions. We will in the following present results from both approaches. However, to be specific we will restrict ourselves here to a discussion of the staggered fermion formulation introduced by Kogut and Susskind [7]. The fermion action can be written as

$$S_F^{KS} = \sum_{nm} Q_{nm}^{KS} \bar{\psi}_n \psi_m; \quad (9)$$

where the staggered fermion matrix  $Q^{KS}$  is given by

$$Q_{nm}^{KS}(\bar{\psi}_q; \sim) = \sum_{\mu=1}^3 (1 - \gamma_\mu) \left( \delta_{n+\hat{\mu}, m} U_{n, \hat{\mu}} + \delta_{n-\hat{\mu}, m} U_{n-\hat{\mu}, \hat{\mu}}^\dagger \right) + \delta_{n, m} \gamma_4 e^{\sim} + \delta_{n, m} \gamma_5 : \quad (10)$$

Here we have introduced the chemical potential  $\sim$  on the temporal links [10]. As the fermion action is quadratic in the Grassmann valued quark fields and we can integrate them out in the partition function and finally arrive at a representation of  $Z(V; T; \sim)$  on a 4-dimensional lattice of size  $N^3 \times N$ ,

$$Z(N; N; \sim; \bar{\psi}_q; \sim) = \int \prod_n dU_n (\det Q^{KS}(\bar{\psi}_q; \sim))^{n_f=4} e^{-S_G} : \quad (11)$$

We have made explicit the fact that the staggered fermion action does lead to four degenerate fermion flavours in the continuum limit, i.e. taking the continuum limit with the action given in Eqs. 9 and 10 corresponds to  $n_f = 4$  in Eq. 11. As the number of fermion species does appear only as an appropriate power of the fermion determinant, which is true also in the continuum limit, one also may choose  $n_f \neq 4$  in Eq. 11. This is the approach used to perform simulations with different number of flavours in the staggered fermion formulation.

For  $\sim = 0$  the fermion determinant appearing in Eq. 11 is real and positive. Standard numerical techniques, which rely on a probability interpretation of the integrand in Eq. 11, thus can be applied. For  $\sim \neq 0$  the determinant, however, becomes complex. Although the contribution of the imaginary part can easily be shown to be zero, as it should to give a real partition function, the real part is no longer strictly positive. This sign problem so far still constitutes a major problem

in the application of numerical techniques to studies of QCD at non-zero baryon number density or non-zero chemical potential. We therefore will restrict our discussion of QCD thermodynamics mainly to the case  $\mu \sim 0$  and will come back to the problems one faces for  $\mu \neq 0$  in Section 8.

## 2.2 ...and back from the lattice to the continuum

The lattice discretized QCD action discussed above reproduces the continuum action up to discretization errors of  $O(a^2)$ . In order to perform the continuum limit at constant temperature, we will have to take the limit  $(a \rightarrow 0; N \rightarrow \infty)$  with  $T = 1/N a$  fixed. In particular, for bulk thermodynamic observables like the pressure and energy density, which have dimension  $[T^4]$  this limit is rather cumbersome. All lattice observables are dimensionless and are thus calculated in appropriate units of the lattice spacing  $a$ . As a consequence a calculation of, e.g., the pressure will provide  $pa^4$  and thus yields a numerical result which decreases in magnitude like  $N^{-4}$ . Numerical calculations, however, are always based on the analysis of a finite set of suitably generated gauge field configurations and thus produce results which have a statistical error. It therefore rapidly becomes difficult to calculate bulk thermodynamic quantities on lattices with large temporal extent  $N$ . For this reason it is of particular importance for finite temperature calculations to be able to use actions which have small discretization errors and thus allow to perform calculations on lattices with moderate temporal extent. Such actions have been developed and successfully applied in thermodynamic calculations for the pure SU(3) gauge theory. In the fermion sector appropriate actions, which reduce cut-off effects in the high temperature ideal gas limit, so far have only been constructed for staggered fermions. As an example we describe a specific choice of improved gauge and staggered fermion actions in more detail in an Appendix.

As mentioned above we have to perform the continuum limit in order to eliminate lattice discretization errors and to arrive finally at quantitative predictions for the QCD thermodynamics. Eventually we thus have to analyze our observables on different size lattices and extrapolate our results to  $N \rightarrow \infty$  at fixed temperature. Unless we perform calculations at a well defined temperature, e.g. the critical temperature, we will have to determine the temperature scale from an additional (zero-temperature) calculation of an observable for which we know its physical value (in MeV). This requires a calculation at the same value of the cut-off (same values of the bare couplings). Of course, we know such a quantity only for the physical case realized in nature, i.e. QCD with two light up and down quark flavours and a heavier strange quark. Nonetheless, we have good reason to believe that certain observables are quite insensitive to changes in the quark masses, e.g. quenched hadron masses<sup>1</sup> ( $m_H$ ) or the string tension ( $\sigma$ ) are believed to be suitable observables to set a physical scale even in the limit of infinite quark masses (pure SU(3) gauge theory). We thus may use calculations of these quantities to define a temperature scale,

$$T = \frac{p}{\sigma} = 1/\sigma N \quad \text{or} \quad T/m_H = 1/m_H N \quad : \quad (12)$$

<sup>1</sup> A physical observable  $O$  is calculated on the lattice as dimensionless quantity, which we denote here by  $\bar{O}$ . Quite often, however, we will also adopt the customary lattice notation, which explicitly specifies the cut-off dependence in the continuum limit, e.g.  $m_H = \bar{m}_H a$  or  $\sim a^2$ .

In the pure SU(3) gauge theory as well as in the massless limit the lattice spacing is controlled through  $\beta$ , the only bare coupling appearing in the Euclidean action. Asymptotically  $\beta$  and  $a$  are then related through the leading order renormalization group equation,

$$\beta_L = \beta_0 - \frac{b_1}{(6\beta_0)^2} e^{-\frac{b_1}{6\beta_0^2}} e^{-\frac{b_2}{6\beta_0^3}}; \quad (13)$$

where the two universal coefficients are given by,

$$\beta_0 = \frac{1}{16\pi^2} (11 - \frac{2}{3}n_f); \quad b_1 = \frac{1}{16\pi^2} (102 - 10 + \frac{8}{3}n_f); \quad (14)$$

and  $\beta_L$  is a scale parameter which unambiguously can be related to the scale parameter in other regularization schemes, e.g. to  $\overline{MS}$ . The continuum limit thus is reached with increasing  $\beta$ .

In the case of non-zero quark masses one has in addition to insure that the continuum limit is taken along a line of constant physics. This can be achieved by keeping a ratio of hadron masses, for instance the ratio of pseudo-scalar and vector meson masses,  $m_{PS} = m_V$ , constant while varying the couplings ( $\beta; m_q$ ). In the limit

$m_q \rightarrow 0$  this requires a tuning of the bare quark masses such that  $m_q \rightarrow 0$ . We also note that for small quark masses the vector meson mass  $m_V$  approaches a constant,  $m_V = m + O(m_q)$ , while the pseudo-scalar is the Goldstone-particle corresponding to the broken chiral symmetry of QCD (pion). Its mass is proportional to the square root of  $m_q$ . In the following we will quite often quote results as a function of  $m_{PS} = m_V$  which is just another way for quoting results for different values of the quark mass.

### 3 The QCD Phase Diagram at Finite Temperature

At vanishing baryon number density (or zero chemical potential) the properties of the QCD phase transition depend on the number of quark flavours and their masses. While it is a detailed quantitative question at which temperature the transition to the high temperature plasma phase occurs, we do expect that the nature of the transition, e.g. its order and details of the critical behaviour, are controlled by global symmetries of the QCD Lagrangian. Such symmetries only exist in the limits of either finite or vanishing quark masses. For any non-zero, finite value of quark masses the global symmetries are explicitly broken. In fact, in the case of QCD the explicit symmetry breaking induced by the finite quark masses is very much similar to that induced by an external ferromagnetic field in spin models. We thus expect that a continuous phase transition, which may exist in the zero or in finite quark mass limit, will turn into a non-singular crossover behaviour for any finite value of the quark mass. First order transitions, on the other hand, may persist for some time before they end in a continuous transition. Whether a true phase transition exists in QCD with the physically realized spectrum of quark masses or whether in this case the transition is just a (rapid) crossover, again becomes a quantitative question which we have to answer through direct numerical calculations.

Our current understanding of the qualitative aspects of QCD phase diagram is based on universality arguments for the symmetry breaking patterns in the heavy [11] as well as the light quark mass regime [12,13]. In the limit of infinitely heavy

quarks, the pure SU(3) gauge theory, the large distance behaviour of the heavy quark free energy,  $F_{qq}$ , provides a unique distinction between confinement below  $T_c$  and deconfinement for  $T > T_c$ . On a lattice of size  $N^3 \times N$  the heavy quark free energy<sup>2</sup> can be calculated from the expectation value of the Polyakov loop correlation function

$$\exp \left( -\frac{F_{qq}(r;T)}{T} \right) = \langle \text{Tr} L_x \text{Tr} L_y^\dagger \rangle ; \quad rT = |x - y|N \quad (15)$$

where  $L_x$  and  $L_y^\dagger$  represent static quark and anti-quark sources located at the spatial points  $x$  and  $y$ , respectively,

$$L_x = \prod_{n=0}^{N-1} U_n ; \quad n = (x_0; \mathbf{x}) : x_0 = 1 \quad (16)$$

For large separations ( $r \gg 1$ ) the correlation function approaches  $\langle \text{Tr} L_i \rangle^2$ , where  $\langle \text{Tr} L_i \rangle = N^{-3} \langle \text{Tr} L_x \rangle$  denotes the Polyakov loop expectation value, which therefore characterizes the behaviour of the heavy quark free energy at large distances and is an order parameter for deconfinement in the SU(3) gauge theory,

$$\langle \text{Tr} L_i \rangle = \begin{cases} 0, & \text{confined phase; } T < T_c \\ > 0, & \text{deconfined phase; } T > T_c \end{cases} \quad (17)$$

The effective theory for the order parameter is a 3-dimensional spin model with global Z(3) symmetry. Universality arguments then suggest that the phase transition is first order in the infinite quark mass limit [11].

In the limit of vanishing quark masses the classical QCD Lagrangian is invariant under chiral symmetry transformations; for  $n_f$  massless quarks the symmetry is

$$U_A(1) \times SU_L(n_f) \times SU_R(n_f).$$

However, only the  $SU(n_f)$  flavour part of this symmetry is spontaneously broken in the vacuum, which gives rise to  $(n_f^2 - 1)$  massless Goldstone particles, the pions. The axial  $U_A(1)$  only is a symmetry of the classical Lagrangian. It is explicitly broken due to quantum corrections in the QCD partition function, the axial anomaly, and therefore gets replaced by a discrete Z( $n_f$ ) symmetry at low temperature. The basic observable which reflects the chiral properties of QCD is the chiral condensate,

$$\langle \bar{\psi} \psi \rangle = \frac{1}{N^3 N} \frac{\partial}{\partial m_q} \ln Z : \quad (18)$$

In the limit of vanishing quark masses the chiral condensate stays non-zero as long as chiral symmetry is spontaneously broken. The chiral condensate thus is an obvious order parameter in the chiral limit,

$$\langle \bar{\psi} \psi \rangle = \begin{cases} > 0, & \text{symmetry broken phase; } T < T_c \\ = 0, & \text{symmetric phase; } T > T_c \end{cases} \quad (19)$$

<sup>2</sup> In the  $T \rightarrow 0$  limit this is just the heavy quark potential; at non-zero temperature  $F_{qq}$  does, however, also include a contribution resulting from the overall change of entropy that arises from the presence of external quark and anti-quark sources.

For light quarks the global chiral symmetry is expected to control the critical behaviour of the QCD phase transition. In particular, the order of the transition is expected to depend on the number of light or massless flavours. The basic aspects of the  $n_f$ -dependence of the phase diagram have been derived by Pisarski and Wilczek [12] from an effective, 3-dimensional Lagrangian for the order parameter<sup>3</sup>,

$$\begin{aligned} \mathcal{L}_{\text{eff}} = & \frac{1}{2} \text{Tr}(\partial_\mu \Sigma \partial^\mu \Sigma^\dagger) - \frac{1}{2} m^2 \text{Tr}(\Sigma) + \frac{g_1}{3} \text{Tr}(\Sigma)^2 \\ & + \frac{g_2}{3} \text{Tr}(\Sigma^\dagger \Sigma)^2 + c (\det \Sigma + \det \Sigma^\dagger) ; \end{aligned} \quad (20)$$

with  $\Sigma = (\sigma_{ij})$ ,  $i, j = 1, \dots, n_f$ .  $\mathcal{L}_{\text{eff}}$  has the same global symmetry as the QCD Lagrangian. A renormalization group analysis of this Lagrangian suggests that the transition is first order for  $n_f \geq 3$  and second order for  $n_f = 2$ . The latter, however, is expected to hold only if the axial  $U_A(1)$  symmetry breaking, related to the determinants in Eq. 20, does not become too weak at  $T_c$  so that the occurrence of a fluctuation induced first order transition would also become possible.

This basic pattern has indeed been observed in lattice calculations. So far no indication for a discontinuous transition has been observed for  $n_f = 2$ . The transition is found to be first order for  $n_f \geq 3$ . Moreover, the transition temperature is decreasing with increasing  $n_f$  and there are indications that chiral symmetry is already restored in the vacuum above a critical number of flavours [15].

The anticipated phase diagram of 3-flavour QCD at vanishing baryon number density is shown in Fig. 1. An interesting aspect of the phase diagram is the occurrence of a second order transition line in the light quark mass regime, the boundary of the region of first order phase transitions. On this line the transition is controlled by an effective 3-dimensional theory with global  $Z(2)$  symmetry [13], which is not a symmetry of the QCD Lagrangian. As this boundary lies in the light quark mass regime it may well be that this second order transition, for which neither the chiral condensate nor the Polyakov loop will be the order parameter, is equally important for the critical or crossover behaviour of QCD with a realistic quark mass spectrum as the nearby critical point in the chiral limit. In particular, we note that the critical exponent  $\beta$  is positive for the 3-d,  $Z(2)$  symmetric models whereas it is negative for the  $O(4)$  model. A nearby  $Z(2)$  symmetric critical point in the QCD phase diagram will thus induce larger density fluctuations than would be expected in the vicinity of the chiral critical point. It therefore will be important to determine in detail the location of the physical point in the QCD phase diagram.

## 4 Deconfinement versus Chiral Symmetry Restoration

As outlined in the previous section the two properties of QCD, which explain the basic features of the observed spectrum of hadrons, are also of central importance for the structure of the QCD phase diagram at finite temperature (confinement and chiral symmetry breaking). While the former explains why we observe only colourless states in the spectrum the latter describes the presence of light Goldstone

<sup>3</sup> It should be noted that this ansatz assumes that chiral symmetry is broken at low temperatures. Instanton model calculations suggest that the vacuum, in fact, is chirally symmetric already for  $n_f \geq 5$  [14].



### 3-flavour phase diagram

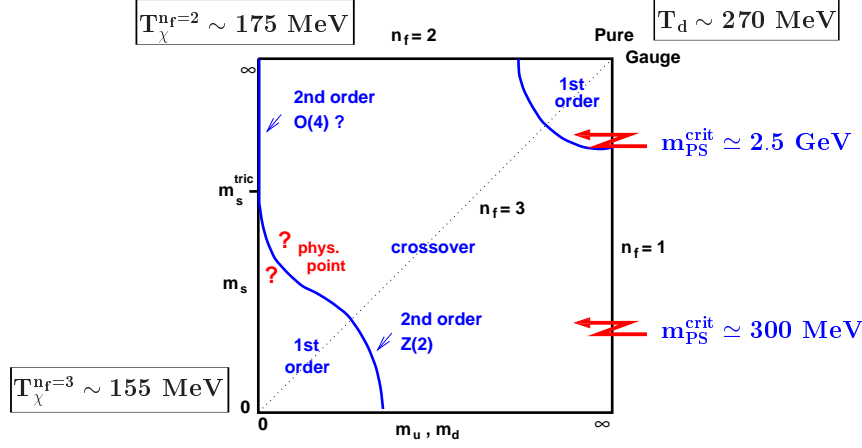


Fig.1. The QCD phase diagram of 3-flavour QCD with degenerate (u,d)-quark masses and a strange quark mass  $m_s$ .

particles, the pions. The confining property of QCD manifests itself in the long range behaviour of the heavy quark potential. At zero temperature the potential rises linearly at large distances<sup>4</sup>,  $V_{qq}(r) \sim r$ , where  $\sigma \sim (425 \text{ MeV})^2$  denotes the string tension, and forces the quarks and gluons to be confined to a hadronic bag. Chiral symmetry breaking leads to a non-vanishing quark anti-quark condensate,  $\langle \bar{q}q \rangle \sim (250 \text{ MeV})^3$  in the vacuum. Inside the hadron bag, however, the condensate vanishes. At high temperatures the individual hadronic bags are expected to merge to a single large bag, in which quarks and gluons can move freely. This bag picture is closely related to percolation models for the QCD phase transition [16]. It provides an intuitive argument for the occurrence of deconfinement and chiral symmetry restoration. A priori it is, however, not evident that both non-perturbative properties have to get lost at the same temperature. It has been speculated that two distinct phase transitions leading to deconfinement at  $T_d$  and chiral symmetry restoration at  $T_{\chi}$  could occur in QCD [17]. General arguments about the scales involved<sup>5</sup> suggest that  $T_d > T_{\chi}$ . Two distinct phase transitions indeed have been found in QCD related models like the SU(3) gauge theory with adjoint fermions [18]. In QCD, however, there seems to be only one transition from the low temperature hadronic regime to the high temperature plasma phase. In fact, as can be seen from Fig. 1 there is a wide range of parameters (quark masses) for which the transition is not related to any singular behaviour in thermodynamic observables; instead of a phase transition one observes just a rapid crossover behaviour. It

<sup>4</sup> Here large distances actually refer to  $r \gg 1 \text{ fm}$ . For larger distances the spontaneous creation of quark anti-quark pairs from the vacuum leads to a breaking of the string, i.e. the potential tends to a constant value for  $r \rightarrow \infty$  (see Fig. 4).

<sup>5</sup> The hadronic bag is larger than the constituent quark bag of a current quark surrounded by its gluon cloud.

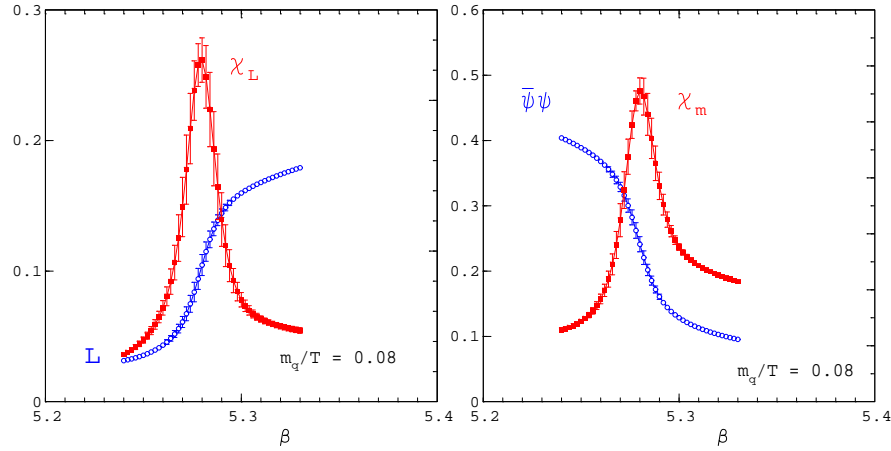


Fig. 2. Deconfinement and chiral symmetry restoration in 2-flavour QCD: Shown is  $L$  (left), which is the order parameter for deconfinement in the pure gauge limit ( $m_q \rightarrow 1$ ), and  $\bar{\psi}\psi$  (right), which is the order parameter for chiral symmetry breaking in the chiral limit ( $m_q \rightarrow 0$ ). Also shown are the corresponding susceptibilities as a function of the coupling  $\beta = 6/g^2$ .

thus is legitimate to ask which thermodynamic properties change when one moves from the low to the high temperature regime and to what extent these changes are related to deconfinement and/or chiral symmetry restoration.

In the previous section we have introduced order parameters for deconfinement in the infinite quark mass limit,  $L$ , and chiral symmetry restoration in the limit of vanishing quark masses,  $\bar{\psi}\psi$ . Related observables, which also signal a sudden change in the long distance behaviour of the heavy quark potential or the chiral condensate as function of temperature, are the corresponding susceptibilities, the Polyakov loop susceptibility ( $\chi_L$ ) and the chiral susceptibility ( $\chi_m$ ),

$$\chi_L = N^3 \frac{\partial^2 L}{\partial \beta^2} ; \quad \chi_m = \frac{\partial}{\partial m_q} \bar{\psi}\psi : \quad (21)$$

The behaviour of these observables is shown in Fig. 2 for the case of two flavour QCD with light quarks. This clearly shows that the gauge coupling at which the different susceptibilities attain their maxima, or correspondingly the points of most rapid change in  $L$  and  $\bar{\psi}\psi$  coincide. Calculations of these observables for QCD with three degenerate quark flavours<sup>6</sup> have been performed for a wide range of quark masses [19]. They confirm that the location of maxima in both susceptibilities are indeed strongly correlated. Within statistical accuracy they occur at the same temperature, although the height of these maxima is strongly quark mass dependent. This is shown in Fig. 3. For large ( $m_{PS} = m_V > 0.9$ ) and small ( $m_{PS} = m_V < 0.3$ ) quark

<sup>6</sup> This corresponds to calculations along the dotted, diagonal line in the phase diagram shown in Fig. 1.

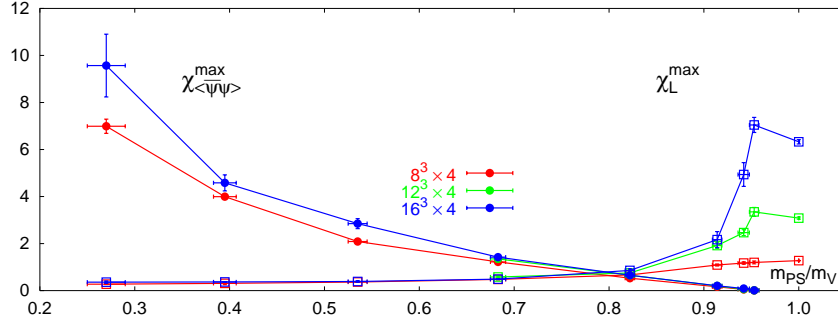


Fig.3. Quark mass dependence of the Polyakov loop and chiral susceptibilities versus  $m_{PS}=m_V$  for 3-flavour QCD. Shown are results from calculations with the improved gauge and staggered fermion action discussed in the Appendix.

masses the Polyakov loop and chiral susceptibility, respectively, show a strong volume dependence, which is indicative for the presence of first order phase transitions in these corners of the phase diagram. Using zero temperature string tension calculations the pseudo-scalar meson masses have been estimated at which the first order transitions end in a second order transition. For better orientation in the phase diagram these estimates, which at present are not well established and certainly are still subject to lattice artifacts (discretization errors, flavour symmetry breaking), are shown in Fig. 1. As can be seen there is a broad range of quark (or meson) masses for which the QCD transition to the high temperature phase is a non-singular crossover.

As expected the first order phase transition in the large quark mass regime is most clearly visible in the behaviour of the Polyakov loop susceptibility, i.e. the fluctuation of the order parameter for the confinement-deconfinement transition in the pure gauge ( $m_q \rightarrow 1$ ) limit. Similarly, the transition in the chiral limit is most pronounced in the behaviour of the chiral condensate and its susceptibility. This emphasizes the chiral aspects of the QCD transition. One thus may wonder in what respect this transition in the light quark mass regime is a deconfining transition.

#### 4.1 Deconfinement

When talking about deconfinement in QCD we have in mind that a large number of new degrees of freedom gets liberated at a (phase) transition temperature; quarks and gluons which at low temperature are confined in colourless hadrons and thus do not contribute to the thermodynamics, suddenly become liberated and start contributing to bulk thermodynamic observables like the energy density or pressure. In the heavy quark mass limit ( $m_q \rightarrow 1$ ) a more rigorous statement is based on the analysis of the long distance behaviour of the heavy quark free energy, which approaches a constant above  $T_c$  but diverges for  $T < T_c$ . For finite quark masses, however, the long distance behaviour of  $F_{qq}$  can no longer serve as an order parameter, the heavy quark free energy stays finite for all temperatures. This is shown in Fig. 4 where we compare results from calculations in the pure

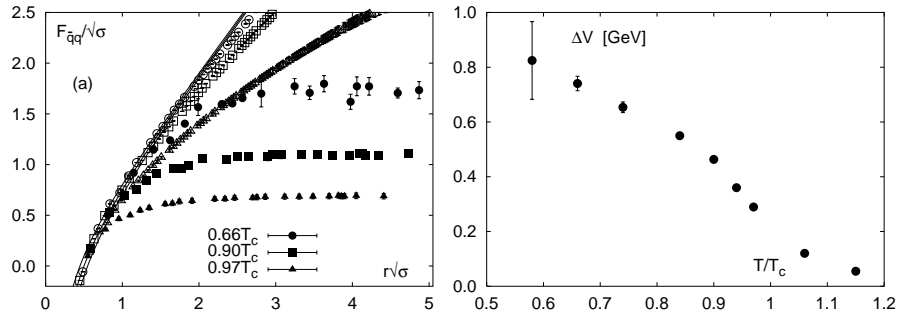


Fig.4. The left hand figure shows the heavy quark free energy in units of the square root of the string tension for the SU (3) gauge theory (open symbols) and three flavour QCD with light quarks (full symbols). The right hand figure gives the limiting value of the free energy normalized to the value at distance  $r = 0.23$  fm [19] as a function of temperature for the case of three flavour QCD. The quark mass used in the  $n_f = 3$  calculations corresponds to a ratio of pseudo-scalar and vector meson masses of  $m_{ps} = m_v = 0.7$ .

gauge theory [20] with results from a calculation in three flavour QCD [19]. It is apparent from this figure that there is no drastic qualitative change in the structure of the heavy quark free energy as one crosses the transition temperature. Although the most rapid change in  $V = F_{qq}(l) - F_{qq}(r = 0.5 \text{ fm})$  occurs for  $T \approx T_c$  and thus resembles the behaviour of the Polyakov loop expectation value and its susceptibility shown in Fig. 2, the heavy quark free energy does not seem to be a good indicator for deconfinement in the presence of light quarks. It loses its role as a rigorous order parameter and also does not reflect changes in the number of partonic degrees of freedom contributing to the thermodynamics.

On the other hand, we expect that bulk thermodynamic quantities like the pressure do reflect the relevant number of degrees of freedom contributing to the thermodynamics in the high temperature limit. Due to asymptotic freedom the QCD pressure will approach the ideal gas value at infinite temperature. In this limit the number of degrees of freedom (quarks+gluons) is much larger than the three light pions which dominate the thermodynamics at low temperature,

$$\frac{p}{T^4} = \begin{cases} \frac{3}{90}, & T \rightarrow 0 \\ (16 + \frac{21}{2}n_f)\frac{1}{90}, & T \rightarrow \infty \end{cases} \quad (22)$$

This change of active degrees of freedom is clearly visible in calculations of e.g. the pressure in the pure gauge sector and for QCD with different numbers of flavours. As can be seen in Fig. 5 the pressure strongly reacts to changes in the number of degrees of freedom. It is this drastic change in the behaviour of the pressure or the energy density which indicates that the QCD (phase) transition to the plasma phase indeed is deconfining. However, it also is worthwhile to note that the transition does, in fact, take place at rather small values of the pressure (and energy density). Only for temperatures  $T > 2T_c$  does the pressure come close to the

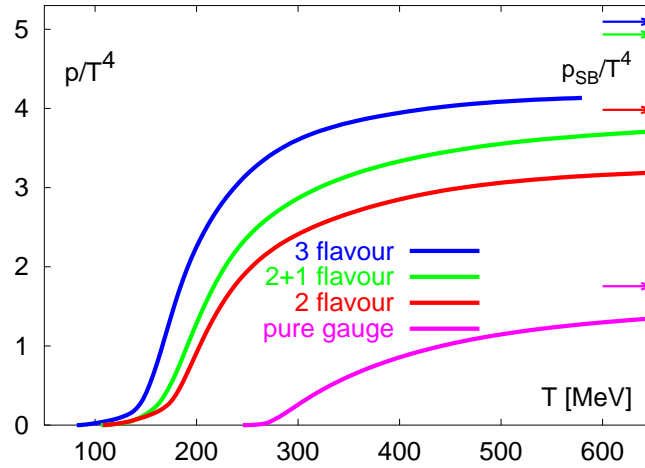


Fig.5. The pressure in QCD with different number of degrees of freedom as a function of temperature. The curve labeled (2+1)-flavour corresponds to a calculation with two light and a four times heavier strange quark mass [21].

ideal gas limit so that one can, with some justification, identify the corresponding light degrees of freedom. This is the case for QCD with light quarks as well as in the quenched limit. At least for temperatures up to a few times  $T_c$  the dynamical degrees of freedom are certainly not just weakly interacting partons.

#### 4.2 Chiral symmetry restoration

As chiral symmetry restoration does not lead to a significant change of light degrees of freedom, it also is not expected to have an appreciable effect on bulk thermodynamic observables (apart from controlling details of the transition very close to  $T_c$ ). In particular, we expect that in the case of a continuous transition for  $n_f = 2$ , the chiral order parameter and its derivative, the chiral susceptibility, show critical behaviour which is characteristic for  $O(4)$  spin models in three dimensions [12]. The expected critical behaviour follows from standard scaling arguments derived from the singular part of the free energy density,

$$f_s(t;h) = \frac{T}{V} \ln Z_s = b^{-d} f_s(b^{y_t} t; b^{y_h} h) ; \quad (23)$$

where  $t = (T - T_c)/T_c$  ( $\tau$ ) is the reduced temperature,  $h = m_q/T$  ( $m_q N$ ) the scaled quark mass and  $b$  is an arbitrary scale factor. For the chiral order parameter,  $\chi$ , and the chiral susceptibility,  $\chi_m$ , one finds from Eq. 23,

$$\chi = h^{1-\beta} F(z) \quad (24)$$

$$\chi_m(t;h) = \frac{1}{h^{1-\beta}} F(z) - \frac{z}{F(z)} F'(z) ; \quad (25)$$

with scaling functions  $F$  and  $F^0$  that only depend on a specific combination of the reduced temperature and scaled quark mass,  $z = t h^{1/\nu}$ . The critical exponents  $\nu$  and  $\beta$  are given in terms of  $\bar{\nu}$  and  $\bar{\beta}$  as  $\nu = (1 - \bar{\nu})/\bar{\nu}$  and  $\beta = \bar{\beta}/\bar{\nu} = (1 - \bar{\beta})/\bar{\nu}$ . As the  $t$ -dependence enters in  $m(t; h)$  only through  $z$  one also deduces that the line of pseudo-critical couplings defined through the location of the maximum of  $m(t; h)$  at fixed  $h$  is described by a universal scaling function,

$$t_c(h) = z_c h^{1/\nu} : \quad (26)$$

Although there is ample evidence that the phase transition in 2-flavour QCD is continuous in the chiral limit, the evidence for the expected  $O(4)$  scaling is, at present, ambiguous. The behaviour of the pseudo-critical couplings is, in general, consistent with the expected scaling behaviour. The information on the magnetic equation of state, Eq. 24, however, seems to depend on the fermion discretization scheme used to analyze the critical behaviour. While calculations with Wilson fermions yield almost perfect agreement with the universal form of the  $O(4)$  magnetic equation of state [22], significant deviations have been found in the case of staggered fermions [23]. The failure of the scaling analysis in the case of staggered fermions is surprising as this staggered fermion action has a global  $O(2)$  symmetry even for finite values of the lattice cut-off and as the  $O(4)$  and  $O(2)$  magnetic equations of state are quite similar [24]. This suggests that finite size effects still play an important role, which is supported by a recent finite size scaling analysis [25]. In Fig. 6 we show the finite size scaling behaviour of the chiral condensate, which has been reanalyzed in [25]. It is consistent with  $O(4)$  (or  $O(2)$ ) scaling behaviour. This aspect, however, clearly needs further studies.

The changes of the chiral condensate below  $T_c$  and chiral symmetry restoration at  $T_c$  will have a strong influence on the light hadron spectrum. At  $T_c$  the pseudo-scalar mesons (pions) will no longer be Goldstone particles, they turn into massive modes (quasi-particle excitations?) above  $T_c$ . Long distance correlations of the chiral condensate decay exponentially with a characteristic length scale proportional to the inverse scalar meson mass. A diverging chiral susceptibility at  $T_c$  thus indicates that the scalar meson mass vanishes at  $T_c$ . The mass splitting between parity partners thus will decrease when the symmetry breaking reduces and finally will become degenerate at  $T_c$ .

As indicated above the modifications of the hadron spectrum are reflected by the temperature dependence of appropriately chosen susceptibilities, which are the space-time integral over hadronic correlation functions in a given quantum number channel,

$$\chi_H = \frac{1}{V} \int_0^T dt \int d^3r G_H(\vec{r}; t) ; \quad (27)$$

where the hadronic correlation function  $G_H(\vec{r}; t)$  for mesons is given by,

$$G_H(\vec{r}; t) = \langle \bar{\psi}(0) \psi(0) (\vec{r}; t) \bar{\psi}(\vec{r}; t) \psi(\vec{r}; t) \rangle ; \quad (28)$$

and  $\bar{\psi}$  is an appropriate combination of  $\psi$ -matrices that projects onto a chosen quantum number channel. In particular, we note that the chiral susceptibility,  $\chi_\sigma$ , defined in Eq. 21 is the susceptibility of the scalar correlation function. These susceptibilities define generalized masses,  $m_H^2 = -\chi_H^{-1}$ , which are shown in Fig. 7. They,

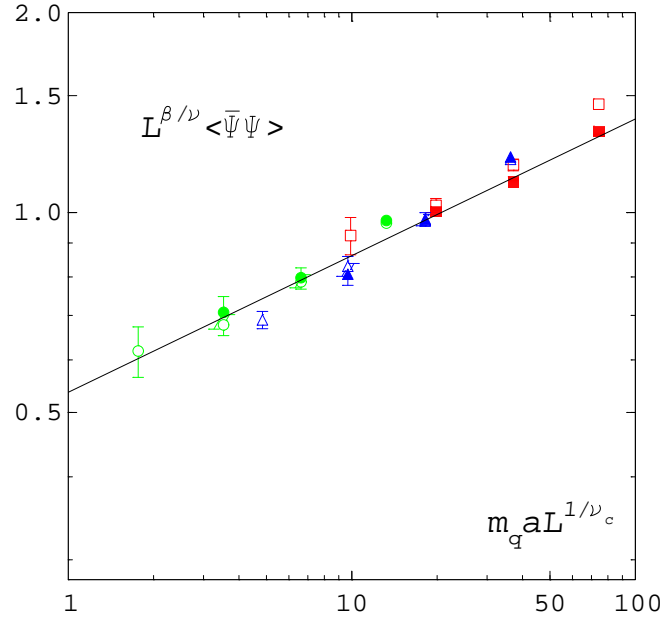


Fig.6. Finite size scaling of the chiral condensate in 2-flavour QCD [25]. Shown are data from calculations with standard staggered fermions on lattices of size  $8^3 \times 4$  (circles),  $12^3 \times 4$  (triangles) and  $16^3 \times 4$  (squares). The calculations have been performed with different values of the quark mass at fixed value of the scaling variable  $z_c$  corresponding to the pseudo-critical line (Eq.26).

indeed, show the expected behaviour; scalar ( $f_0$ ) and pseudo-scalar ( $\pi$ ) partners become degenerate at  $T_c$  whereas the vector meson ( $\rho$ ) which is related to the scalar meson through a  $U_A(1)$  rotation only gradually approaches the other masses. The axial  $U_A(1)$  symmetry thus remains broken at  $T_c$ .

## 5 Screening at High Temperature { Short versus Long Distance Physics

Our picture of the thermodynamics in the high temperature phase of QCD largely is influenced by perturbative concepts { asymptotic freedom and the screening of electric and magnetic components of the gluon fields. Asymptotic freedom suggests that the temperature dependent running coupling,  $g(T)$ , becomes small at high temperatures and eventually vanishes in the limit  $T \rightarrow \infty$ . This in turn will lead to a separation of the thermal length scale,  $1=T$ , from the electric,  $1=g(T)T$ , and magnetic,  $1=g^2(T)T$ , screening length scales. The experience gained from lattice calculations in the pure SU(3) gauge theory, however, suggests that this separation of scales, unfortunately, will set in only at asymptotically large temperatures. For all interesting temperatures reachable in heavy ion experiments or even covering the temperature interval between the strong and electroweak phase transitions that

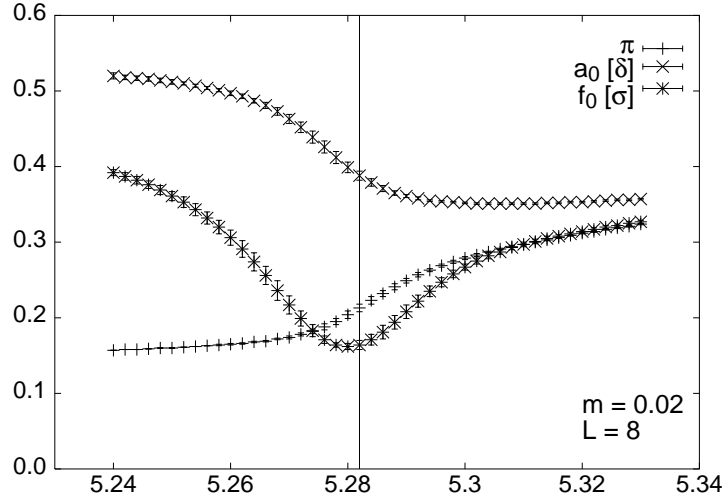


Fig.7. Temperature dependence of generalized hadron masses extracted from hadronic susceptibilities. Shown are results from calculations in 2-flavour QCD performed on lattices of size  $8^3 \times 4$  with staggered fermions of mass  $m_q = 0.02$ .

occurred in the early universe, the coupling  $g(T)$  is of  $O(1)$  and, moreover, the Debye screening mass is significantly larger than the leading order perturbative value,

$$m_D = \frac{g}{1 + \frac{n_f}{6} g(T) T} \quad (29)$$

In fact, for  $T_c < T < 100 T_c$  one finds that  $m_D$  is still about three times larger than this leading order value [26]. A consequence of this large value of the screening mass is that also short distance properties of the plasma are strongly influenced by non-perturbative screening effects; the Debye screening length,  $r_D = 1/m_D$ , becomes compatible with the characteristic length scale  $r_{SB}$  in a free gas where the main contribution to the Stefan-Boltzmann law originates from particle with momenta  $p \sim 3T$ , i.e.  $r_{SB} = 1/3T$ , and is of the same order as the mean separation between partons in a quark-gluon plasma. We thus must expect that non-perturbative screening effects also have an influence on bulk thermodynamics properties (pressure, energy density) above  $T_c$  and even up to quite large temperatures. In fact, the calculations of the pressure and energy density in the  $SU(3)$  gauge theory and in QCD with light quarks, which we are going to discuss in the next section, show that at temperatures a few times  $T_c$  deviations from the ideal gas limit are still too large to be understood in terms of conventional high temperature perturbation theory, which converges badly at these temperatures just because of the large contribution arising from Debye screening [30].

The screening of static quark and anti-quark sources is commonly analyzed in terms of Polyakov-loop correlation functions, which define the heavy quark free energy introduced in Eq. 15. The leading perturbative contribution to  $F_{qq}(r; T)$



results from the exchange of two gluons,

$$\begin{aligned} \frac{V_{qq}(r;T)}{T} - \frac{F_{qq}(r;T)}{T} - F_{qq}^1 &= -\ln \frac{hT r L_x T r L_y i}{jL i^2} \\ &= \frac{1}{16} \frac{g^2(T)}{3} \frac{1}{rT} + O(g^5) : \end{aligned} \quad (30)$$

Higher order contributions will lead to screening of this powerlike large distance behaviour,  $1/rT \rightarrow \exp(-m_D r)/rT$ , and also result in an exponentiation of the leading order contribution. We then may split  $F_{qq}$  in contributions arising from quark anti-quark pairs in singlet ( $F_1$ ) and octet ( $F_8$ ) configurations [3],

$$e^{-F_{qq}(r;T)/T} = \frac{1}{9} e^{-F_1(r;T)/T} + \frac{8}{9} e^{-F_8(r;T)/T} : \quad (31)$$

In accordance with zero temperature perturbation theory the singlet free energy is attractive whereas the octet free energy is repulsive. Their relative strength is such that it leads to a cancellation of the leading  $O(g^2)$  contributions to the colour averaged heavy quark free energy  $F_{qq}$ . From Eq. 31 it is, however, apparent, that the cancellation of singlet and octet contributions only occurs at large distances. At short distances the contribution from the attractive singlet channel will dominate the heavy quark free energy,

$$\begin{aligned} \frac{F_{qq}(r;T)}{T} &= \frac{F_1(r;T)}{T} + \text{const} : \\ &= \frac{g^2(T)}{3} \frac{1}{rT} + \text{const} : \quad \text{for } rT \ll 1 : \end{aligned} \quad (32)$$

In order to eliminate the subleading power-like behaviour at large distances we show in Fig. 8  $(rT)^2 V_{qq}(r;T)/T$  calculated for the SU(3) gauge theory. As can be seen the change from the Coulomb-like behaviour at short distances to the exponential screening at large distances can be well localized. For  $T_c \leq T < 2T_c$  it occurs already for  $rT \approx 0.2$  or  $r \approx 0.15 (T_c/T)$  fm and shifts slightly to smaller  $rT$  with increasing temperature. A consequence of this efficient screening at short distances is that even heavy quark bound states get destroyed close to  $T_c$  in the plasma phase (J = - suppression [28]).

The perturbative analysis of the heavy quark free energy also suggests that for fixed  $rT$  the only temperature dependence of  $V(r;T)/T$  arises from the running of the coupling  $g(T)$ . The rapid change of  $V(r;T)/T$  at fixed  $rT$  which is apparent in Fig. 8 thus also suggests that for temperatures  $T < 3T_c$  the coupling  $g(T)$  varies much more rapidly than the asymptotically expected logarithmic running with  $T$ .

We thus conclude that non-perturbative screening effects are important for the thermodynamics in the plasma phase also for short distance observables which are sensitive to the physics at distances  $r \gtrsim 1-5T$ . The strong temperature dependence observed for  $T < 3T_c$ , moreover, suggests that the system cannot be described at a weakly coupled, asymptotically free plasma at these temperatures. These general features will carry over to the temperature dependence of the QCD equation of state which we are going to discuss in the next section.

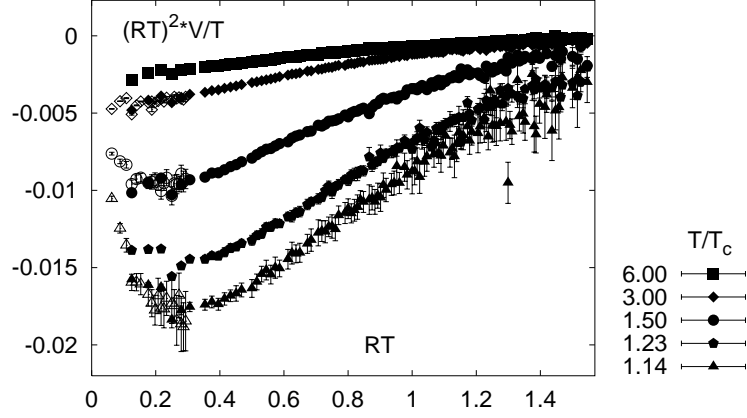


Fig.8. The heavy quark free energy at various temperatures in the deconfined phase of the SU (3) gauge theory. Calculations have been performed on lattices of size  $32^3$   $\times$  8 (filled symbols) and  $32^3$   $\times$  16 (open symbols) [27].

## 6 The QCD Equation of State

The most fundamental quantity in equilibrium thermodynamics is, of course, the partition function itself, or the free energy density,

$$f = -\frac{T}{V} \ln Z(T; V) \quad (33)$$

All basic bulk thermodynamic observables can be derived from the free energy density. In the thermodynamic limit we obtain directly the pressure,  $p = -f$  and subsequently also other quantities like the energy ( $\epsilon$ ) and entropy ( $s$ ) densities or the velocity of sound ( $c_s$ ),

$$\frac{\epsilon}{T^4} = T \frac{d}{dT} \left( \frac{p}{T^4} \right) \quad ; \quad \frac{s}{T^3} = \frac{\epsilon + p}{T^4} \quad ; \quad c_s^2 = \frac{dp}{d\epsilon} \quad (34)$$

In the limit of infinite temperature asymptotic freedom suggests that these observables approach the ideal gas limit for a gas of free quarks and gluons,  $\epsilon = 3p = \frac{3}{4}f$  with  $p = T^4$  given by Eq. 22. Deviations from these ideal gas values have been studied in high temperature perturbation theory. However, it was well-known that this expansion is no longer calculable perturbatively at  $O(g^6)$  [29]. By now all calculable orders up to  $O(g^5 \ln g)$  have been calculated [30]. Unfortunately it turned out that the information gained from this expansion is rather limited. The expansion shows bad convergence behaviour and suggests that it is of use only at temperatures several orders of magnitude larger than the QCD transition temperature. In analytic approaches one thus has to go beyond perturbation theory which currently is being attempted by either using hard thermal loop resummation techniques [31,32] or perturbative dimensional reduction combined with numerical simulations of the resulting effective 3-dimensional theory [33].

In order to make use of the basic thermodynamic relations, Eqs. 33 and 34, in numerical calculations on the lattice we have to go through an additional intermediate step. The free energy density itself is not directly accessible in Monte Carlo calculations; e.g. only expectation values can be calculated easily. One thus proceeds by calculating differences of the free energy density at two different temperatures. These are obtained by taking a suitable derivative of  $\ln Z$  followed by an integration, e.g.

$$\frac{f}{T^4} \Big|_{T_0}^T = \frac{1}{V} \int_{T_0}^T dx \frac{\partial x^{-3} \ln Z(x; V)}{\partial x} : \quad (35)$$

This ansatz readily translates to the lattice. Taking derivatives with respect to the gauge coupling,  $\beta = 6/g^2$ , rather than the temperature as was done in Eq. 35, we obtain expectation values of the Euclidean action which can be integrated again to give the free energy density,

$$\frac{f}{T^4} \Big|_{T_0}^T = N^4 \int_{T_0}^T d\beta \langle H_S \rangle - \langle H_S \rangle_{T=0} : \quad (36)$$

Here

$$\langle H_S \rangle = \frac{1}{N^3 N} \frac{\partial \ln Z}{\partial \beta} ; \quad (37)$$

is calculated on a lattice of size  $N^3 \times N$  and  $\langle H_S \rangle_{T=0}$  denotes expectation values calculated on zero temperature lattices, which usually are approximated by symmetric lattices with  $N^4$ . The lower integration limit is chosen at low temperatures so that  $f|_{T_0}^T$  is small and may be ignored<sup>7</sup>.

A little bit more involved is the calculation of the energy density as we have to take derivatives with respect to the temperature,  $T = 1/\beta a$ . On lattices with fixed temporal extent  $N$  we rewrite this in terms of a derivative with respect to the lattice spacing  $a$  which in turn is controlled through the bare couplings of the QCD Lagrangian,  $\beta = \beta(a; m_q)$ . We thus find for the case of  $n_f$  degenerate quark flavours of mass  $m_q$

$$\begin{aligned} \frac{\epsilon}{T^4} &= N^4 \frac{d \langle H \rangle}{d \ln a} - \langle H \rangle_{T=0} \\ &\quad - \frac{dm_q(a)}{d \ln a} \langle H \rangle_{T=0} : \end{aligned} \quad (38)$$

An evaluation of the energy density thus e.g. requires the knowledge of two functions. These may be determined by calculating two physical observables in

<sup>7</sup> In the gluonic sector the relevant degrees of freedom at low temperature are glueballs. Even the lightest ones calculated on the lattice have large masses,  $m_G \sim 1.5 \text{ GeV}$ . The free energy density thus is exponentially suppressed already close to  $T_c$ . In QCD with light quarks the dominant contribution to the free energy density comes from pions. As long as we are dealing with massive quarks also this contribution gets suppressed exponentially. However, in the massless limit clearly some care has to be taken with the normalization of the free energy density.

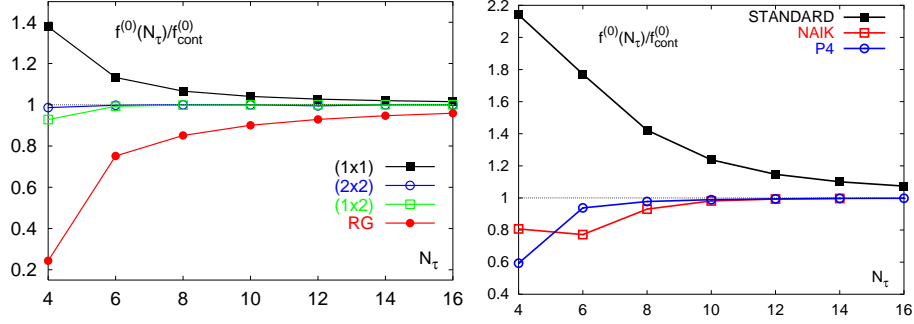


Fig.9. Cut-off dependence of the ideal gas pressure for the SU (3) gauge theory (left) and several staggered fermion actions (right). These actions are defined in the Appendix. Cut-off effects for the Wilson fermion action are compatible with those of the standard staggered fermion action.

lattice units for given values of  $\beta$  and  $m_q$ ; for instance, the string tension,  $\sigma a^2$  and a ratio of hadron masses,  $m_{PS}/m_V = m/m$ . These quantities will have to be calculated at zero temperature which then also allows to determine a temperature scale in physical units as given in Eq. 12. This forms the basis for a calculation of the pressure as shown already in Fig. 5.

The numerical calculation of thermodynamic quantities is done on finite lattices with spatial extent  $N_s$  and temporal extent  $N_t$ . In order to perform calculations close to the thermodynamic limit we want to use a large spatial extent of the lattice. In general it has been found that lattices with  $N_s > 4N_t$  provide a good approximation to the infinite volume limit. In addition, we want to get close to the continuum limit in order to eliminate discretization errors. Taking the continuum limit at fixed temperature requires to perform the limit  $N_t \rightarrow \infty$ . In order to perform this limit in a controlled way we have to analyze in how far lattice calculations of bulk thermodynamic observables are influenced by the introduction of a finite lattice cut-off, i.e. we have to understand the systematic cut-off effects introduced through the non-zero lattice spacing. These cut-off effects are largest in the high (infinite) temperature limit which can be analyzed analytically in weak coupling lattice perturbation theory. We thus will discuss this limiting case first.

### 6.1 High temperature limit of the QCD equation of state

In the high temperature limit bulk thermodynamic observables are expected to approach their free gas values (Stefan-Boltzmann constants). In this limit cut-off effects in the pressure and in turn also in the energy density ( $\epsilon_{SB} = 3 p_{SB}$ ) become most significant. Moments of the order of the temperature, i.e. short distance properties, dominate the ideal gas behaviour.

As discussed in Section 2 the most straightforward lattice representation of the QCD partition function in terms of the standard Wilson gauge and fermion actions as well as the staggered fermion action leads to a systematic  $O(a^2)$  cut-off dependence of physical observables. At finite temperature the temperature itself

sets the scale for these  $O(a^2)$  effects, which thus give rise to  $O((aT)^2 - 1/N^2)$  deviations of e.g. the pressure from the continuum Stefan-Boltzmann value,

$$\frac{P}{T^4} = \frac{P}{T^4} + \frac{C}{N^2} + O(N^{-4}) : \quad (39)$$

One can eliminate these leading order cut-off effects by using improved actions which greatly reduces the cut-off dependence in the ideal gas limit. In the Appendix we discuss a specific set of improved gauge and fermion actions. In the gauge sector one may in addition to the standard Wilson plaquette term  $(1-1)$ -action) also include planar 6-link terms in the action. This is done in the  $O(a^2)$  tree level improved  $(1-2)$ -action, which eliminates the leading order cut-off dependence completely. On lattices with temporal extent  $N$  one finds for the deviation of the gluonic part of the pressure [34],

$$\frac{p_G(N)}{p_{G,SB}} = \begin{cases} 1 + \frac{8}{21} \frac{1}{N^2} + \frac{5}{21} \frac{1}{N^4} + O(N^{-6}) & , (1-1)\text{-action} \\ 1 + O(N^{-4}) & , (1-2)\text{-action} \end{cases} \quad (40)$$

A similar reduction of cut-off effects can be achieved in the fermion sector through the use of improved actions. So far, however, improved fermion actions, which reduce or eliminate the leading order cut-off effects have only been constructed in the staggered fermion formulation. The Naik action [35], which in addition to the ordinary one-link term in the staggered action also includes straight three-link terms, completely eliminates the  $O(N^{-2})$  errors on the tree level (ideal gas limit). The p4-action discussed in the Appendix does not eliminate this correction completely. It, however, reduces its contribution drastically over those present in the standard staggered action<sup>8</sup>,

$$\frac{p_F(N)}{p_{F,SB}} = \begin{cases} < 1 + 1.57 \frac{1}{N^2} + 8.47 \frac{1}{N^4} + O(N^{-6}) & , 1\text{-link standard} \\ : 1 + 0.007 \frac{1}{N^2} + 1.07 \frac{1}{N^4} + O(N^{-6}) & \text{staggered action} \\ & , p4\text{-action} \end{cases} \quad (41)$$

as can be seen in Fig. 9. Moreover, the p4-action has the advantage that it improves the rotational symmetry of the fermion propagator which in turn also reduces violations of rotational symmetry in the heavy quark potential.

Using the tree level improved gauge action in combination with the improved staggered fermion action in numerical simulations at finite temperature it is possible to perform calculations with small systematic cut-off errors already on lattices with small temporal extent, e.g.  $N_t = 4$  or 6. In actual calculations performed with various actions in the pure gauge sector one finds that for temperatures  $T < 5T_c$  the cut-off dependence of thermodynamic shows the pattern predicted by the infinite temperature perturbative calculation. The absolute magnitude of the cut-off effects, however, is smaller by about a factor of two. This, of course, is reassuring for the numerical calculations performed with light quarks, where such a detailed systematic study of the cut-off dependence at present does not exist.

<sup>8</sup> We quote here only an approximation to the  $N$ -dependence obtained from a fit in the interval  $10 \leq N \leq 16$ .

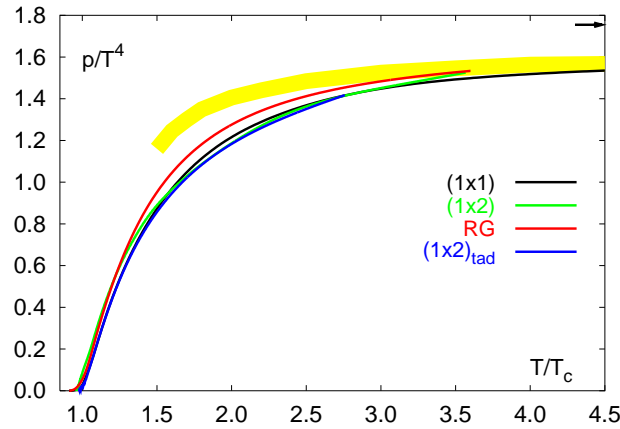


Fig. 10. Pressure of the SU (3) gauge theory calculated on lattices with different temporal extent and extrapolated to the continuum limit. Shown are results from calculations with the standard Wilson (1 1)-action [36] and several improved actions [38,39], which are defined in the Appendix. The broad band shows the approximately self-consistent HTL calculation of [41].

## 6.2 Thermodynamics of the SU (3) gauge theory

Before entering a discussion of bulk thermodynamics in two and three flavour QCD it is worthwhile to discuss some results on the equation of state in the heavy quark mass limit of QCD – the SU (3) gauge theory. In this case the temperature dependence of the pressure and energy density has been studied in great detail, calculations with the standard action [36] and various improved actions [37,38,39] have been performed, the cut-off dependence has explicitly been analyzed through calculations on lattices with varying temporal extent  $N_t$  and results have been extrapolated to the continuum limit. In Fig. 10 we show some results for the pressure obtained from such detailed analyses with different actions [36,38,39]. This figure shows the basic features of the temperature dependence of bulk thermodynamic quantities in QCD, which also carry over to the case of QCD with light quarks. The pressure stays small for almost all temperatures below  $T_c$ ; this is expected, as the only degrees of freedom in the low temperature phase are glueballs which are rather heavy and thus lead to an exponential suppression of pressure and energy density at low temperature. Above  $T_c$  the pressure rises rapidly and reaches about 70% of the asymptotic ideal gas value at  $T = 2 T_c$ . For even larger temperatures the approach to this limiting value proceeds rather slowly. In fact, even at  $T \sim 4 T_c$  deviations from the ideal gas value are larger than 10%. This is too much to be understood in terms of weakly interacting gluons as they are described by ordinary high temperature perturbation theory [30]. Even at these high temperatures non-perturbative effects have to be taken into account which may be described in terms of interactions among quasi-particles [31,40]. In Fig. 10 we show the result of a self-consistent HTL resummation [41], which leads to good agreement with

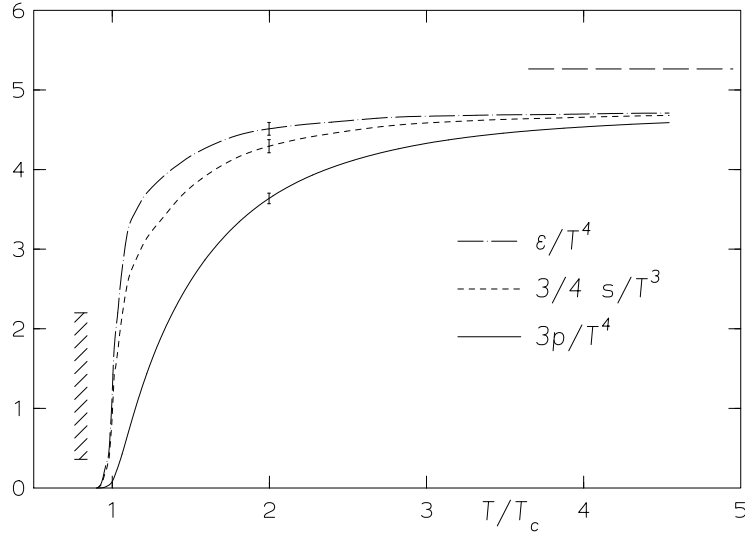


Fig.11. Energy density, entropy density and pressure of the SU (3) gauge theory calculated on lattices with different temporal extent and extrapolated to the continuum limit. The dashed band indicates the size of the latent heat gap in energy and entropy density

the lattice calculations for  $T > 3T_c$ . Other approaches [33,40] reach a similarly good agreement in the high temperature regime.

Compared to the pressure the energy density rises much more rapidly in the vicinity of  $T_c$ . In fact, as the transition is first order in the SU (3) gauge theory the energy density is discontinuous at  $T_c$  with a latent heat of about  $1.5T_c^4$  [42]. In Fig. 11 we show results for the energy density, entropy density and the pressure obtained from calculations with the Wilson action which have been extrapolated to the continuum limit [36]. The delayed rise of the pressure compared to that of the energy density has consequences for the velocity of sound in the QCD plasma in the vicinity of  $T_c$ . It is substantially smaller than in the high temperature ideal gas limit.

### 6.3 Flavour dependence of the QCD equation of state

As shown in Eq. 36 the pressure in QCD with light quarks can be calculated along the same line as in the pure gauge sector. Unlike in the pure gauge case it, however, will be difficult to perform calculations on lattices with large temporal extent. In fact, at present all calculations of the equation of state are restricted to lattices with  $N_t = 4$  and 6 [21,43,44]. The use of an improved fermion action thus seems to be even more important in this case. Of course, an additional problem arises from insufficient chiral properties of staggered and Wilson fermion actions. This will mainly be of importance in the low temperature phase and in the vicinity of the transition temperature. The continuum extrapolation thus will be more involved in

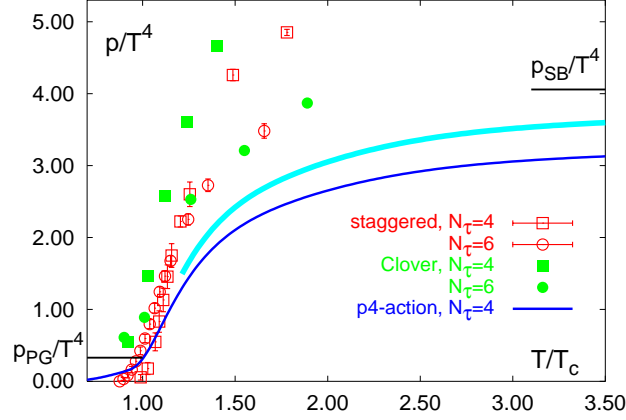


Fig. 12. The pressure in two flavour QCD calculated with unimproved gauge and staggered fermion actions (open symbols) [43], RG-improved gauge and clover improved Wilson action (full symbols) [44] and the p4-action (improved gauge and improved staggered fermions, see Appendix) (full line) [21]. The dashed band estimates the results in the continuum limit as described in the text. The horizontal lines to the right and left show the Stefan-Boltzmann values for an ideal pion gas and a free quark-gluon gas, respectively.

the case of QCD with light quarks than in the pure gauge theory and we will have to perform calculations closer to the continuum limit. Nonetheless, in particular for small number of flavours, we may expect that the flavour symmetry breaking only has a small effect on the overall magnitude of bulk thermodynamic observables. After all, for  $n_f = 2$ , the pressure of an ideal massless pion gas contributes less than 10% of that of an ideal quark-gluon gas in the high temperature limit. For our discussion of bulk thermodynamic observables the main source for lattice artifacts thus still seems to arise from the short distance cut-off effects, which we have to control. Additional confidence in the numerical results can be gained by comparing simulations performed with different fermion actions.

The importance of an improved lattice action, which leads to small cut-off errors at least in the high temperature ideal gas limit is apparent from Fig. 12, where we compare the results of a calculation of the pressure in 2-flavour QCD performed with unimproved gauge and staggered fermion actions [43] and the RG-improved gauge and clover improved Wilson action [44] with results obtained with the p4-action discussed in the Appendix. At temperatures above  $T \approx 2 T_c$  these actions qualitatively reproduce the cut-off effects calculated analytically in the infinite temperature limit (see Section 6.1). In particular, it is evident that also the Clover improved Wilson action leads to an overshooting of the continuum ideal gas limit. This is expected as the Clover term in the Wilson action does eliminate  $O(a g^2)$  cut-off effects but does not improve the high temperature ideal gas limit, which is  $O(g^0)$ . The clover improved Wilson action thus leads to the same large  $O(a^2)$  cut-off effects as the unimproved Wilson action. The influence of cut-off effects in bulk thermodynamic



observables thus is similar in calculations with light quarks and in the SU(3) gauge theory. This observation may also help to estimate the cut-off effects still present in current calculations with light quarks. In particular, we know from the analysis performed in the pure gauge sector that in the interesting temperature regime of a few times  $T_c$  the cut-off dependence seems to be about a factor two smaller than calculated analytically in the infinite temperature limit; we may expect that this carries over to the case of QCD with light quarks. This is the basis for the estimated continuum extrapolation of the  $n_f = 2$  results shown as a dashed band in Fig. 12.

In Fig. 5 we have already shown results for the pressure calculated in QCD with different number of flavours. This figure clearly shows that the transition region shifts to smaller temperatures as the number of degrees of freedom is increased. Such a conclusion, of course, requires the determination of a temperature scale that is common to all QCD-like theories which have a particle content different from that realized in nature. We have determined this temperature scale by assuming that the string tension is flavour and quark mass independent. This assumption is supported by the observation that already in the heavy quark mass limit the string tension calculated in units of quenched hadron masses, e.g.  $m_{\pi}^{\text{P}} = 1.81(4)$  [45], is in good agreement with values required in QCD phenomenology,  $m_{\pi}^{\text{P}} \approx 425 \text{ MeV}$ .

At high temperature the magnitude of  $p/T^4$  clearly reflects the change in the number of light degrees of freedom present in the ideal gas limit. When we rescale the pressure by the corresponding ideal gas values it becomes, however, apparent that the overall pattern of the temperature dependence of  $p/T^4$  is quite similar in all cases. This is shown in Fig. 13. In particular, when one takes into account that a proper continuum extrapolation in QCD with light quarks is still missing this agreement achieved with improved staggered fermions is quite remarkable.

We also note that the pressure at low temperature is enhanced in QCD with light quarks compared to the pure gauge case. This is an indication for the contribution of hadronic states, which are significantly lighter than the heavy glueballs of the SU(3) gauge theory. This behaviour is even more clearly visible in the behaviour of the energy density which is shown in Fig. 14, where we show results obtained with improved staggered<sup>9</sup> and Wilson [44] fermions. We note that these calculations yield consistent estimates for the energy density at  $T_c$ ,

$$\epsilon_c \approx (6 \pm 2) T_c^4 : \quad (42)$$

This estimate for  $\epsilon_c = T_c^4$ , which also is consistent with results obtained from calculations with a standard staggered fermion action [43], is an order of magnitude larger than the critical value on the hadronic side of the transition in the pure gauge theory (see Fig. 11). It is, however, interesting to note that when we convert this result for  $\epsilon_c$  in physical units,  $[\text{MeV}/\text{fm}^3]$ , this difference gets to a large extent compensated by the shift in  $T_c$  to smaller values. When going from the infinite quark mass limit to the light quark mass regime the QCD transition thus seems to take place at compatible values of the energy density,  $\epsilon_c \approx (0.5 \pm 0.1) \text{ GeV}/\text{fm}^3$ . The largest uncertainty on this number at present arises from uncertainties on the value of  $T_c$  (see next section). However, also the magnitude of  $\epsilon_c = T_c^4$  still has to be determined more accurately. Here two competing effects will be relevant. On the

<sup>9</sup> The figure for staggered fermions is based on data from Ref. [21]. Here a contribution to  $\epsilon = T^4$  which is proportional to the bare quark mass and vanishes in the chiral limit is not taken into account.

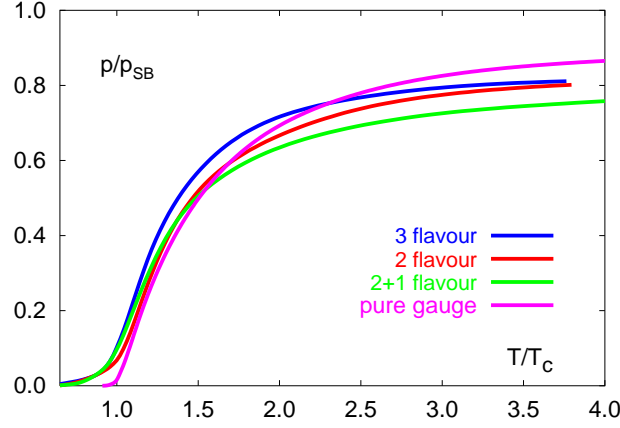


Fig. 13. The pressure in units of the ideal gas pressure for the SU (3) gauge theory and QCD with various number of flavours. The latter calculations have been performed on lattices with temporal extent  $N_t = 4$  using the p4-action defined in the Appendix. Results are not yet extrapolated to the continuum limit.

one hand we expect  $\epsilon_c = T_c^4$  to increase with decreasing quark masses, i.e. closer to the chiral limit. On the other hand, it is likely that finite volume effects are similar to those in the pure gauge sector, which suggests that  $\epsilon_c = T_c^4$  will still decrease closer to the thermodynamic limit, i.e. for  $N_t \rightarrow \infty$ .

In the 2-flavour calculations performed with improved Wilson fermions [44] the pressure and energy density have been calculated for several values of the quark mass, which corresponds to different ratios of the pseudo-scalar to vector meson mass  $m_{PS} = m_V$ . The results show no significant quark mass dependence up to  $m_{PS} = m_V \approx 0.9$ . This meson mass ratio corresponds to pseudo-scalar meson masses of about 1.5 GeV, which is somewhat larger than the  $\pi$ -meson mass. This suggests that the corresponding quark mass is compatible with that of the strange quark. The approximate quark mass independence of the equation of state observed in the high temperature phase thus is consistent with our expectation that quark mass effects should become significant only when the quark masses get larger than the temperature.

## 7 The Critical Temperature of the QCD Transition

As discussed in Section 3 the transition to the high temperature phase is continuous and non-singular for a large range of quark masses. Nonetheless, for all quark masses this transition proceeds rather rapidly in a small temperature interval. A definite transition point thus can be identified, for instance through the location of peaks in the susceptibilities of the Polyakov loop or the chiral condensate defined in Eq. 21. For a given value of the quark mass one thus determines pseudo-critical couplings,  $\beta_{pc}(m_q)$ , on a lattice with temporal extent  $N_t$ . An additional calculation of an

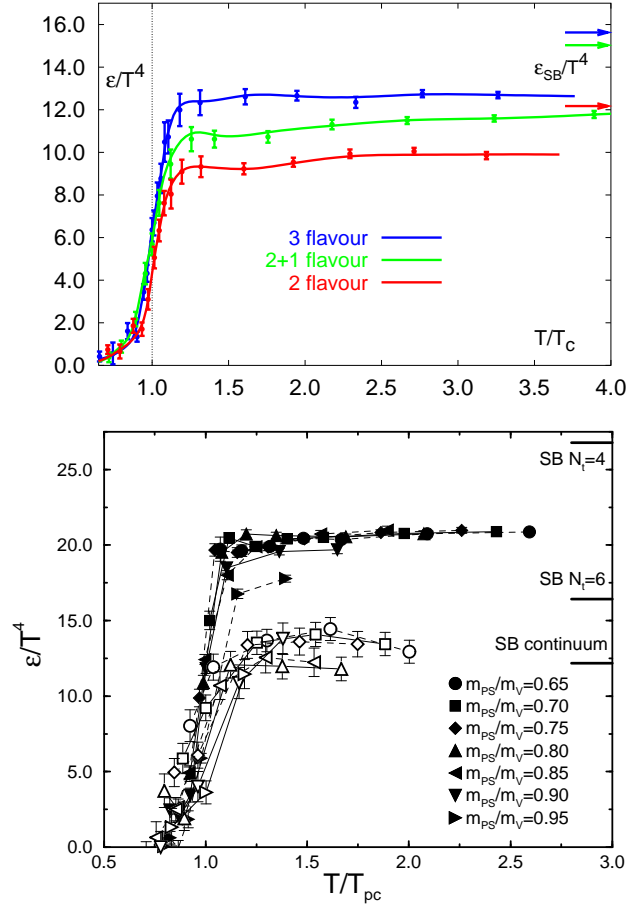


Fig.14. The energy density in QCD. The upper (lower) figure shows results from a calculation with improved staggered [21] (Wilson [44]) fermions on lattices with temporal extent  $N_t = 4$  ( $N_t = 4; 6$ ). The staggered fermion calculations have been performed for a pseudo-scalar to vector meson mass ratio of  $m_{PS}/m_V = 0.7$ .

experimentally or phenomenologically known observable at zero temperature, e.g. a hadron mass or the string tension, is still needed to determine the transition temperature from Eq. 12. In the pure gauge theory the transition temperature, again has been analyzed in great detail and the influence of cut-off effects has been examined through calculations on different size lattices and with different actions. From this one finds for the critical temperature of the first order phase transition in the pure SU (3) gauge theory,

$$\text{SU (3) gauge theory : } T_c^{\text{P}} = 0.637 \pm 0.005$$

$$T_c = (271 \pm 2) \text{ MeV} \quad (43)$$

Already the early calculations for the transition temperature with light quarks [46,47] indicated that the inclusion of light quarks leads to a significant decrease of the transition temperature. However, these early calculations, which have been performed with standard Wilson [46] and staggered [47] fermion actions, also led to significant discrepancies in the results for  $T_c$  as well as the order of the transition. These differences strongly diminished in the newer calculations which are based on improved Wilson fermions (Clover action) [47,48,49], domain wall fermions [50] as well as improved staggered fermions (p4-action) [19]. A compilation of these newer results is shown in Fig. 15 for various values of the quark masses. In order to compare calculations performed with different actions the results are presented in terms of a physical observable, the meson mass ratio  $m_{PS}=m_V$ . In Fig. 15a we show  $T_c=m_V$  obtained for 2-flavour QCD while Fig. 15b gives a comparison of results obtained with improved staggered fermions [19] for 2 and 3-flavour QCD. Also shown there is a result for the case of (2+1)-flavour QCD, i.e. for two light and one heavier quark flavour degree of freedom. Unfortunately the quark masses in this latter case are still too large to be compared directly with the situation realized in nature. We note however, that the results obtained so far suggest that the transition temperature in (2+1)-flavour QCD is close to that of 2-flavour QCD. The 3-flavour theory, on the other hand, leads to consistently smaller values of the critical temperature,  $T_c(n_f=2) \sim T_c(n_f=3) \sim 20$  MeV. The extrapolation of the transition temperatures to the chiral limit gave

$$\begin{array}{ll}
 \begin{array}{l} 2 \\ \hline 2 \end{array} \text{ flavour QCD} : T_c = & \begin{array}{l} 8 \\ \gtrsim \\ 171 \end{array} \text{ (4) MeV ; } \begin{array}{l} \text{clover-improved Wilson} \\ \text{fermions [48]} \end{array} \\
 \begin{array}{l} 3 \\ \hline 3 \end{array} \text{ flavour QCD} : T_c = & \begin{array}{l} 8 \\ \gtrsim \\ 173 \end{array} \text{ (8) MeV ; } \begin{array}{l} \text{improved staggered} \\ \text{fermions [19]} \end{array} \\
 \begin{array}{l} 3 \\ \hline 3 \end{array} \text{ flavour QCD} : T_c = & (154 \text{ } 8) \text{ MeV ; } \begin{array}{l} \text{improved staggered} \\ \text{fermions [19]} \end{array}
 \end{array}$$

Here  $m_V$  has been used to set the scale for  $T_c$ . Although the agreement between results obtained with Wilson and staggered fermions is striking, one should bear in mind that all these results have been obtained on lattice with temporal extent  $N_t = 4$ , i.e. at rather large lattice spacing,  $a \sim 0.3$  fm. Moreover, there are uncertainties involved in the ansatz used to extrapolate to the chiral limit. We thus estimate that the systematic error on the value of  $T_c=m_V$  still is of similar magnitude as the purely statistical error quoted above.

We note from Fig. 15 that  $T_c=m_V$  drops with increasing ratio  $m_{PS}=m_V$ , i.e. with increasing quark mass. This may not be too surprising as  $m_V$ , of course, does not take on the physical meson mass value as long as  $m_{PS}=m_V$  did not reach its physical value (vertical line in Fig. 15a). In fact, we know that  $T_c=m_V$  will approach zero for  $m_{PS}=m_V = 1$  as  $T_c$  will stay finite and take on the value calculated in the pure SU(3) gauge theory whereas  $m_V$  will diverge in the heavy quark mass limit. Fig. 15 thus does not yet allow to quantify how  $T_c$  depends on the quark mass. A simple percolation picture for the QCD transition would suggest that  $T_c(m_q)$  or better  $T_c(m_{PS})$  will increase with increasing  $m_q$ ; with increasing  $m_q$  also the hadron masses increase and it becomes more difficult to excite the low lying hadronic states. It thus becomes more difficult to create a sufficiently high particle/energy density in the hadronic phase that can trigger a phase (percolation) transition. Such a picture also follows from chiral model calculations [51].

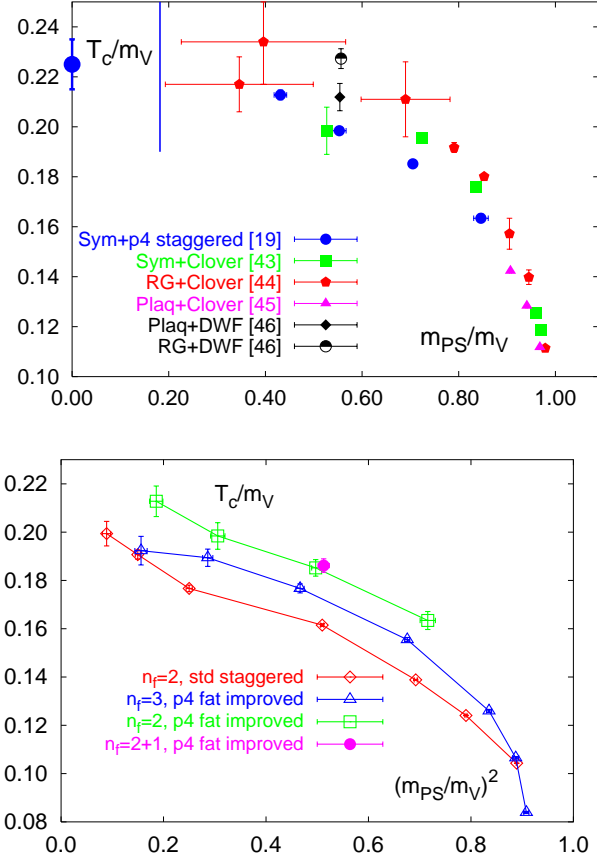


Fig.15. Transition temperatures in units of  $m_V$ . The upper figure shows a collection of results obtained for 2-flavour QCD with various fermion actions while in the lower figure we compare results obtained in 2 and 3-flavour QCD with the p4-action described in the Appendix. All results are from simulations on lattices with temporal extent  $N_t = 4$ . The large dot drawn for  $m_{PS} = m_V = 0$  indicates the result of chiral extrapolations based on calculations with improved Wilson [48] as well as improved staggered [19] fermions. The vertical line in the upper figure shows the location of the physical limit,  $m_{PS} = m = 140 \text{ MeV}$ .

As argued previously we should express  $T_c$  in units of an observable, which itself is not dependent on  $m_q$ ; the string tension (or also a quenched hadron mass) seems to be suitable for this purpose. In fact, this is what tacitly has been assumed when one converts the critical temperature of the  $SU(3)$  gauge theory  $T_c = \frac{p}{0.63}$  into physical units as has also been done in Eq. 43.

To quantify the quark mass dependence of the transition temperature one may express  $T_c$  in units of  $\frac{p}{m_V}$ . This ratio is shown in Fig. 16 as a function of  $m_{PS} = \frac{p}{m_V}$ . As can be seen the transition temperature starts deviating from the quenched values for

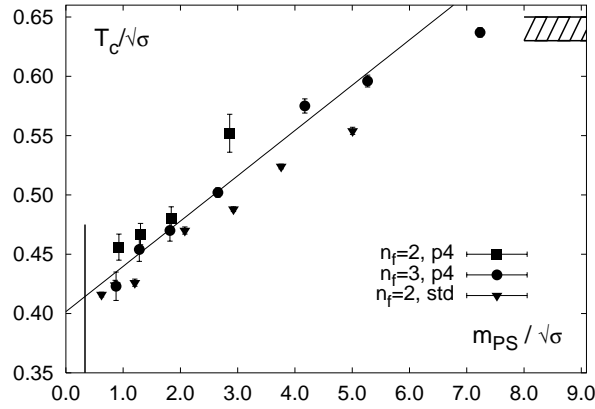


Fig.16. The transition temperature in 2 (filled squares) and 3 (circles) flavour QCD versus  $m_{PS} = \frac{P}{\sqrt{\sigma}}$  using an improved staggered fermion action (p4-action). Also shown are results for 2-flavour QCD obtained with the standard staggered fermion action (open squares). The dashed band indicates the uncertainty on  $T_c = \frac{P}{\sqrt{\sigma}}$  in the quenched limit. The straight line is the fit given in Eq. 45.

$m_{PS} < (6-7) \frac{P}{\sqrt{\sigma}} \approx 2.5 \text{ GeV}$ . We also note that the dependence of  $T_c$  on  $m_{PS} = \frac{P}{\sqrt{\sigma}}$  is almost linear in the entire mass interval. Such a behaviour might, in fact, be expected for light quarks in the vicinity of a  $2^{\text{nd}}$  order chiral transition where the dependence of the pseudo-critical temperature on the mass of the Goldstone-particle follows from the scaling relation, Eq. 26,

$$T_c(m) - T_c(0) \propto m^{2-\beta} : \quad (44)$$

For 2-flavour QCD the critical indices are expected to belong to the universality class of 3-d, O(4) symmetric spin models and one thus would indeed expect  $1-\beta = 0.55$ . However, this clearly cannot be the origin of the quasi-linear behaviour which is observed for rather large hadron masses and seems to be independent of  $n_f$ . Moreover, unlike in chiral models [51] the dependence of  $T_c$  on  $m_{PS}$  turns out to be rather weak. The line shown in Fig. 16 is a fit to the 3-flavour data, which gave

$$\frac{T_c}{\frac{P}{\sqrt{\sigma}}} = \frac{T_c}{\frac{P}{\sqrt{\sigma}}} \Big|_{m_{PS}=0} + 0.04(1) \frac{m_{PS}}{\frac{P}{\sqrt{\sigma}}} : \quad (45)$$

It thus seems that the transition temperature does not react strongly on changes of the lightest hadron masses. This favours the interpretation that the contributions of heavy resonance masses are equally important for the occurrence of the transition. In fact, this also can explain why the transition still sets in at quite low temperatures even when all hadron masses, including the pseudo-scalars, attain masses of the order of 1 GeV or more. Such an interpretation also is consistent with the weak quark mass dependence of the critical energy density we found from the analysis of the QCD equation of state in the previous section.

For the quark masses currently used in lattice calculations a resonance gas model combined with a percolation criterion thus provides an appropriate to describe the thermodynamics close to  $T_c$ . It remains to be seen whether the role of the light meson sector becomes more dominant when we get closer to the chiral limit.

## 8 Finite Density QCD

Finite density calculations in QCD are affected by the wellknown sign problem, i.e. the fermion determinant appearing in the QCD partition function, Eq. 11, becomes complex for non-zero values of the chemical potential and thus prohibits the use of conventional numerical algorithms. The most detailed studies of this problem have so far been performed using the Glasgow algorithm [52], which is based on a fugacity expansion of the grand canonical partition function at non-zero ,

$$Z_{GC}(\mu; T; V) = \sum_{B=0}^{\infty} \frac{z^B}{B!} Z_B(T; V); \quad (46)$$

where  $z = \exp(\mu/T)$  is the fugacity and  $Z_B$  are the canonical partition functions for fixed quark number  $B$ ;  $B = 3, 6$  for one species of staggered or Wilson fermions, respectively. After introducing a complex chemical potential in  $Z_{GC}$  the canonical partition functions can be obtained via a Fourier transformation<sup>10</sup>,

$$Z_B(T; V) = \frac{1}{2\pi} \int_{-\infty}^{\infty} d\mu e^{i\mu B} Z_{GC}(i\mu; T; V) \quad (47)$$

$$= \int \prod_n dU_n \prod_B a_B e^{-S_G}; \quad (48)$$

with

$$a_B = \frac{1}{2\pi} \int_{-\infty}^{\infty} d\mu e^{i\mu B} (\det Q^F(m_q; i\mu))^{n_F/4}; \quad (49)$$

One thus may evaluate the canonical partition functions as expectation values with respect to a trial partition function that can be handled numerically, for instance the partition function of the pure SU(3) gauge theory,

$$Z_{GC}(\mu; T; V) = Z_{SU(3)} \sum_{B=0}^{\infty} \frac{z^B}{B!} \langle n_B \rangle_{SU(3)}; \quad (50)$$

However, this approach so far did not overcome the severe numerical difficulties. Like other approaches it suffers from the problem that expectation values have to be calculated with respect to another ensemble so that the importance sampling

<sup>10</sup> The use of this ansatz for the calculation of canonical partition functions as expansion coefficients for  $Z_{GC}$  has been discussed in [55,56]. A new approach has been suggested recently, which combines simulations with imaginary chemical potential with an analytic continuation based on the Ferrenberg-Swendsen multi-histogram method [57].

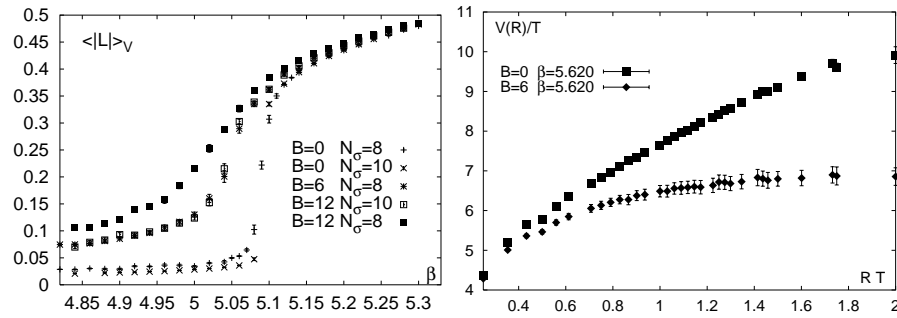


Fig. 17. Polyakov loop expectation value (left) calculated on  $N^3 = 2$  and the heavy quark potential (right) calculated on  $16^3 \times 4$  lattices in quenched QCD at zero and non-zero baryon number,  $B=3$ .

which is at the heart of every numerical approach samples the wrong region of phase space and thus may become quite inefficient.

It thus may be helpful to approach the finite density problems from another perspective. A reformulation of the original ansatz may lead to a representation of the partition function which, in the ideal case, would require the averaging over configurations with strictly positive weights only, or at least would lead to a strong reduction of configurations with negative weights.

An alternative formulation of finite density QCD is given in terms of canonical rather than grand canonical partition functions [53], i.e. rather than introducing a non-zero chemical potential through which the number density is controlled one introduces directly a non-zero baryon number (or quark number  $B$ ) through Eq. 47 from which the baryon number density on lattices of size  $N^3 \times N$  is obtained as  $n_B = T^3 = \frac{B}{3} (N - N^{-1})^3$ . Also this formulation is by no means easy to use in general, i.e. for QCD with light quarks. In particular, it also still suffers from a sign problem. It, however, leads to a quite natural and useful formulation of the quenched limit of QCD at non-zero density [54] which may be a good starting point for generalizing this approach to finite values of the quark mass. In the following we briefly outline the basic ideas of this approach.

### 8.1 Quenched limit of finite density QCD

It had been noticed early that the straightforward replacement of the fermion determinant by a constant does not lead to a meaningful static limit of QCD [58]. In fact, this simple replacement corresponds to the static limit fermion flavours carrying baryon number  $B$  and  $-B$ , respectively [59]. This should not be too surprising. When one starts with QCD at a non-zero baryon number and takes the limit of infinitely heavy quarks something should be left over from the determinant that represents the objects that carry the baryon number. In the canonical formulation this becomes obvious. For  $m_q \rightarrow \infty$  one ends up with a partition function, which for baryon number  $B=3$  still includes the sum over products of  $B$  Polyakov loops, i.e. the static quark propagators which carry the baryon number [54]. This limit



also has some analogy in the grand canonical formulation where the coupled limit  $m_q \rightarrow \infty$  with  $\exp(\beta) = 2m_q$  kept fixed has been performed [60,61]<sup>11</sup>.

As the baryon number is carried by the rather heavy nucleons in the condensed phase of QCD we may expect that it is quite reasonable to approximate them by static objects. This may already provide valuable insight into the thermodynamics of QCD at non-zero baryon number density already from quenched QCD.

In the canonical approach simulations at non-zero  $B$  can be performed on relatively large lattices and the use of baryon number densities up to a few times nuclear matter density is possible [54,62]. The simulations performed so far in the static limit show the basic features expected at non-zero density. As can be seen from the behaviour of the Polyakov loop expectation value shown in Fig. 17 the transition region gets shifted to smaller temperatures (smaller coupling). The broadening of the transition region suggests a smooth crossover behaviour at non-zero density. However, in a canonical simulation it also may indicate the presence of a region of coexisting phases and thus would signal the existence of a 1<sup>st</sup> order phase transition. This deserves further analysis.

Even more interesting is the behaviour of the heavy quark free energy in the low temperature phase. As shown in the right frame of Fig. 17 the free energy does get screened at non-vanishing number density. The influence of static quark sources on the heavy quark free energy is similar in magnitude to the screening (string breaking) seen in QCD simulations at finite temperature in the low temperature hadronic phase (see Fig. 4). At non-zero baryon number density we thus may expect similarly strong medium effects as at finite temperature.

## 9 Conclusions

We have given a brief introduction into the lattice formulation of QCD thermodynamics and presented a few of the basic results on the QCD equation of state, the critical parameters for the transition to the QCD plasma phase and properties of this new phase of matter.

The thermodynamics of the heavy quark mass limit is quite well under control; we know the equation of state and the transition temperature with an accuracy of a few percent. We now also have reached a first quantitative understanding of QCD with light quarks, which at present still corresponds to a world in which the pion would have a mass of about (300-500) MeV. This still is too heavy to become sensitive to details of the physics of chiral symmetry breaking. Nonetheless, lattice calculations performed with different lattice fermion formulations start to produce a consistent picture for the quark mass dependence of the equation of state as well as the influence of the number of light flavours on the phase transition and they yield compatible results for the transition temperature. In these calculations we learn to control the systematic errors inherent to lattice calculations performed with a finite lattice cut-off and start getting control over the effects resulting from the explicit

<sup>11</sup> This is a well known limit in statistical physics. When deriving the non-relativistic gas limit from a relativistic gas of particles with mass  $m$ , the rest mass is splitted off from the chemical potential,  $\mu \rightarrow \mu - m$ , in order to cancel the corresponding rest mass term in the particle energies. On the lattice  $m = \ln(2m_q)$  for large bare quark masses.

breaking of continuum symmetries in the fermion sector. With these experience at hand we soon will be able to study the thermodynamics of QCD with a realistic spectrum of light up and down quarks and a heavier strange quark.

## Acknowledgement

I would like to thank the organizers of the 40th Schlading Winter School on "Dense Matter" for arranging a very stimulating topical meeting. Furthermore, I would like to thank all my colleagues in Bielefeld, in particular Jurgen Engels, Edwin Laermann, Bengt Petersson and Helmut Satz, for the extremely fruitful collaboration I had with them for many years on most of the topics discussed in these lectures.

## Appendix: Improved Gauge and Fermion Actions

### Improved gauge actions

When formulating a discretized version of QCD one has a great deal of freedom in choosing a lattice action. Different formulations may differ by sub-leading powers of the lattice cut-off, which vanish in the continuum limit. This has, for instance, been used by Symanzik to systematically improve scalar field theories [63] and has then been applied to lattice regularized SU(N) gauge theories [64,65]. In addition to the elementary plaquette term appearing in the standard Wilson formulation of lattice QCD larger loops can be added to the action in such a way that the leading  $O(a^2g^0)$  deviations from the continuum formulation are eliminated and corrections only start in  $O(a^4g^0; a^2g^2)$ . A simple class of improved actions is, for instance, obtained by adding planar loops of size (k;l) to the standard Wilson action (one-plaquette action) [34]. The simplest extension of the Wilson one-plaquette action thus is to include an additional contribution from a planar six-link Wilson loop,

$$W_{n,i}^{(1;2)} = \frac{1}{6} \operatorname{Re} \left[ \text{Diagram 1} + \text{Diagram 2} \right]_{n,i} \quad (51)$$

Combining this six-link contribution with the four-link plaquette term in a suitable way one can eliminate the leading  $O(a^2)$  corrections and arrives at a formulation that reproduces the continuum action up to  $O(a^4)$  corrections at least on the classical level at  $O(g^0)$ ,

$$S_G = \sum_{0 \leq n \leq 3} c_{1,1} W_{n,i}^{(1;1)} + c_{1,2} W_{n,i}^{(1;2)} \quad ; \quad (52)$$

with  $c_{1,1} = 5/3$  and  $c_{1,2} = 1/6$ . We call this action the tree-level improved (1-2)-action. It may be further improved perturbatively by eliminating the leading lattice cut-off effects also at  $O(g^2)$ , i.e.  $c_{i,j} \rightarrow c_{i,j}^{(0)} + g^2 c_{i,j}^{(1)}$ , or by introducing non-perturbative modifications. A well-studied gluon action with non-perturbative corrections is the RG-improved action introduced by Y. Iwasaki [66]. This RG-action also has the structure of Eq. 52 but with coefficients  $c_{1,1}^{RG} = 3.648$  and

$c_{1,2}^{RG} = 0.662$ . Of course, this action will still lead to  $O(a^2)$  corrections in the ideal gas limit. The  $N$ -dependence of cut-off effects resulting from these actions is shown in Fig. 9. In Section 6 we also show some results from calculations with a tadpole improved action [67]. This non-perturbative improvement amounts to  $c_{1,1}^{tad} = c_{1,1}$  and a replacement of  $c_{1,2}$  by  $c_{1,2}^{tad} = 1 + 6u_0^2$  where,

$$u_0^4 = \frac{1}{6N^3 N} \sum_{x; >}^X (1 - W^{1,1}_i(x)) \quad (53)$$

In the ideal gas limit this action still has the same cut-off dependence as the tree-level improved (1-2) action.

#### Improved staggered fermion actions

When discussing the improvement of fermion actions there are at least two aspects one has to take into account. On the one hand one faces problems with cut-off effects similar to the pure gauge sector; on the tree level the standard Wilson and Kogut-Susskind discretization schemes introduce  $O(a^2)$  which will influence the short distance properties of physical observables. On the other hand also the global symmetries of the continuum Lagrangian are explicitly broken at non-zero lattice spacing. This influences the long distance properties of these actions, e.g. the light particle sector (Goldstone modes) of the lattice regularized theory. Both aspects are of importance for thermodynamic calculations. The latter problem certainly is of importance in the vicinity of the QCD phase transition while the former will show up when analyzing the high temperature limit of the equation of state.

In the case of staggered fermions both problems have been addressed and schemes have been developed that lead to a reduction of cut-off effects at short distances, i.e. high temperature, and also allow to reduce the explicit flavour symmetry breaking of the staggered discretization scheme.

A particular form of improved action used in recent calculations of the Bielefeld group is a staggered fermion action, which in addition to the standard one-link term includes a set of bended three-link terms,

$$\begin{aligned}
 S_F(m_q) = & c_1^F S_{1-link;fat} + c_3^F S_{3-link} + m_q \sum_x \bar{\psi}_x \psi_x \\
 & + \sum_x \bar{\psi}_x \left( \frac{3}{8} \sum_y \frac{q}{y} \frac{b-q}{x-y} + \frac{1}{96} \sum_y \left[ \begin{array}{c} \text{bent three-link terms} \end{array} \right] \right) \psi_x
 \end{aligned}$$

$$+ m_q \sum_x \bar{\psi}_x \psi_x : \quad (54)$$

Here  $(\psi_x) = (1)^{x_0 + i x_1 + j x_2 + k x_3}$  denotes the staggered fermion phase factors. Furthermore, we have made explicit the dependence of the fermion action on different quark flavours  $q$ , and the corresponding bare quark masses  $m_q$ , and give an intuitive graphical representation of the action. The tree level coefficients  $c_1^F$  and  $c_3^F$  appearing in  $S_F$  have been fixed by demanding rotational invariance of the free quark propagator at  $O(p^4)$  ("p4-action") [69]. In addition the 1-link term of the fermion action has been modified by introducing "fat" links [68] with a weight  $\omega = 0.2$ . The use of fat links does lead to a reduction of the flavour symmetry breaking close to  $T_c$  and at the same time does not modify the good features of the p4-action at high temperature, i.e. it does not modify the cut-off effects at tree level and has little influence on the cut-off dependence of bulk thermodynamic observables at  $O(g^2)$  in the high temperature phase [69]. Further details on the definition of the action are given in [69].

We refer to this action with a fat 1-link term combined with the tree level improved gauge action as the p4-action. The  $N_f$ -dependence of cut-off effects resulting from this action is shown in Fig. 9.

## References

1. K.G.Wilson, Phys. Rev. D 10, 2445 (1974);  
K.G.Wilson, in New Phenomena In Subnuclear Physics, Part A, Proceedings of the International School of Subnuclear Physics, Erice, 1975, ed. A. Zichichi, Plenum Press, New York 1977.
2. M.Creutz, Phys. Rev. D 21, 2308 (1980).
3. L.D.McLerran and B. Svetitsky, Phys. Lett. B 98, 195 (1981) and Phys. Rev. D 24, 450 (1981).
4. J.Kuti, J. Polonyi and K. Szlachanyi, Phys. Lett. B 98, 199 (1981).
5. J. Engels, F. Karsch, I. Montvay and H. Satz, Phys. Lett. B 101, 89 (1981).
6. F. Wilczek, Back to basics at ultrahigh temperatures, Physics Today, April 1998, p.11
7. J. Kogut and L. Susskind, Phys. Rev. D 11, 395 (1975).
8. D.B.Kaplan, Phys. Lett. B 288, 342 (1992).
9. P. Chen et al., The finite temperature QCD phase transition with domain wall fermions, hep-lat/0006010.
10. F. Karsch and P. Hasenfratz, Phys. Lett. 125B, 308 (1983).
11. B. Svetitsky and L.G. Ya, Nucl. Phys. B 210 [FS6], 423 (1982).
12. R.D. Pisarski and F. Wilczek, Phys. Rev. D 29, 338 (1984).
13. S. Gavin, A. Gocksch, and R.D. Pisarski, Phys. Rev. D 49, 3079 (1994).
14. E. Shuryak and T. Schaefer, Phys. Rev. Lett. 75, 1707 (1995).
15. Y. Iwasaki, K. Kanaya, S. Sakai and T. Yoshie, Nucl. Phys. (Proc. Suppl.) B 42, 261 (1995).
16. H. Satz, Nucl. Phys. A 642 (1998) 130.
17. E. Shuryak, Phys. Lett. B 107 (1981) 103.
18. F. Karsch and L. Lütgemeier, Nucl. Phys. B 550 (1999) 449.
19. F. Karsch, E. Laermann and A. Peikert, Quark Mass and Flavour Dependence of the QCD Phase Transition, hep-lat/0012023, to appear in Nucl. Phys. B.

20. O. Kaczmarek, F. Karsch, E. Laermann and M. Lutgemeier, Phys. Rev. D 62 (2000) 034021.
21. F. Karsch, E. Laermann and A. Peikert, Phys. Lett. B 478, 447 (2000).
22. Y. Iwasaki, K. Kanaya, S. Kaya and T. Yoshie, Phys. Rev. Lett. 78, 179 (1997).
23. C. Bernard et al. (MILC Collaboration), Phys. Rev. D 61, 054503 (2000).
24. J. Engels, S. Holtmann, T. Mendes and T. Schulze, Phys. Lett. B 492, 219 (2000).
25. J. Engels, S. Holtmann, T. Mendes and T. Schulze, Finite-size scaling functions for 3d O(4) and O(2) spin models and QCD, hep-lat/0105028.
26. K. Kajantie et al., Phys. Rev. Lett. 79, 3130 (1997).
27. O. Kaczmarek, F. Karsch, P. Petreczky and F. Zantow, in preparation.
28. T. Matsui and H. Satz, Phys. Lett. B 178, 416 (1986).
29. A. D. Linde, Phys. Lett. B 96, 289 (1980).
30. P. Arnold and C.-X. Zhai, Phys. Rev. D 50, 7603 (1994);  
B. Kastening and C. Zhai, Phys. Rev. D 52 (1995) 7232.
31. J.-P. Blaizot, E. Iancu and A. Rebhan, Phys. Rev. Lett. 83, 2906 (1999).
32. for a review see J.-P. Blaizot, E. Iancu, hep-ph/0101103; for further details see also the contributions of J.-P. Blaizot and A. Rebhan to this volume.
33. K. Kajantie, M. Laine, K. Rummukainen and Y. Schroder, Phys. Rev. Lett. 86, 10 (2001).
34. B. Beinlich, F. Karsch and E. Laermann, Nucl. Phys. B 462, 415 (1996).
35. S. Naik, Nucl. Phys. B 316 (1989) 238.
36. G. Boyd et al., Phys. Rev. Lett. 75, 4169 (1995) and Nucl. Phys. B 469, 419 (1996).
37. A. Papa, Nucl. Phys. B 478, 335 (1996).
38. M. Okamoto et al. (CP-PACS), Phys. Rev. D 60, 094510 (1999).
39. B. Beinlich et al., Eur. Phys. J. C 6, 133 (1999).
40. A. Peshier, B. Kampfer, O. P. Pavlenko, and G. So, Phys. Rev. D 54, 2399 (1996);  
P. Levai and U. Heinz, Phys. Rev. C 57, 1879 (1998).
41. J.-P. Blaizot, E. Iancu and A. Rebhan, Phys. Lett. B 470, 181 (1999).
42. B. Beinlich, F. Karsch and A. Peikert, Phys. Lett. B 390, 268 (1997).
43. C. Bernard et al., Phys. Rev. D 55, 6861 (1997).
44. A. Ali Khan et al. (CP-PACS), Equation of state in finite temperature QCD with two flavors of improved Wilson quarks, hep-lat/0103028.
45. H. Wittig, Int. J. Mod. Phys. A 12, 4477 (1997).
46. K. M. Bitar et al., Phys. Rev. D 43, 2396 (1991).
47. C. Bernard et al., Phys. Rev. D 56, 5584 (1997) and references therein.
48. A. Ali Khan et al. (CP-PACS), Phys. Rev. D 63, 034502 (2001).
49. R. G. Edwards and U. M. Heller, Phys. Lett. B 462, 132 (1999).
50. N. Christ, private communication.
51. H. Meyer-Ottmanns and B.-J. Schaefer, Phys. Rev. D 53, 6586 (1996);  
J. Berges, D. J. Jungnickel and C. Wetterich, Phys. Rev. D 59, 034010 (1999).
52. I. M. Barbour et al., Nucl. Phys. B (Proc. Suppl.) 60A (1998) 220.
53. D. E. Miller and K. Redlich, Phys. Rev. D 35 (1987) 2524.
54. J. Engels et al., hep-lat/9903030.
55. A. Hasenfratz and D. Toussaint, Nucl. Phys. B 371 (1992) 539 and references therein.
56. M. Alford et al., Phys. Rev. D 59 (1999) 054502.

57. Z.Fodor and S.D.Katz, A new method to study QCD at finite temperature and chemical potential, hep-lat/0104001.
58. I.Barbour et al., Nucl.Phys.B 275, 296 (1986).
59. M.A.Stephanov, Phys.Rev.Lett. 76, 4472 (1996).
60. I.Bender, Nucl.Phys.B (Proc.Suppl.) 26, 323 (1992).
61. T.Blum, J.E.Hetrick and D.Toussaint, Phys.Rev.Lett. 76, 1019 (1996).
62. J.Engels, O.Kaczmarek, F.Karsch and E.Laermann, Nucl.Phys.B 558, 307 (1999) and ERRATUM Nucl.Phys.B 576, 657 (2000).
63. K.Symanski, Nucl.Phys.B 226, 187 (1983) and Nucl.Phys.B 226, 205 (1983).
64. P.Weisz, Nucl.Phys.B 212, 1 (1983); P.Weisz and R.Wohlert, Nucl.Phys.B 236, 397 (1984) and Nucl.Phys.B 247, 544 (1984).
65. M.Luscher and P.Weisz, Comm.Math.Phys. 97, 59 (1985).
66. Y.Iwasaki, Nucl.Phys.B 258, 141 (1985) and Univ.of Tsukuba report UTHEP-118 (1983).
67. G.P.Lepage and P.B.Mackenzie, Phys.Rev.D 48, 2250 (1993).
68. T.Blum, C.DeTar, S.Gottlieb, K.Rummukainen, U.H.Heller, J.E.Hetrick, D.Toussaint, R.L.Sugar and M.Wingate, Phys.Rev.D 55 (1997) 1133.
69. U.M.Heller, F.Karsch and B.Sturm, Phys.Rev.D 60 (1999) 114502.